UNIVERSITÀ DEGLI STUDI DI PADOVA

Dipartimento di Fisica e Astronomia "Galileo Galilei"

Corso di Laurea Magistrale in Fisica

Tesi di Laurea

Cosmological Aspects of Fuzzy Dark Matter

Relatore

Prof. Sabino Matarrese

Correlatore

Prof. Matteo Viel

Laureando

Giulio Romanelli

Anno Accademico 2017/2018

[This page intentionally left blank]

Contents

1 Introduction

Currently, among the theories that describe the Universe on a large scale, the ΛCDM Model is the most widely accepted by the scientific community. It describes a spatially-flat Universe, in which the energy is allocated as follows:

- $68 \pm 1\%$ in Dark Energy
- $27 \pm 1\%$ in Dark Matter
- $\sim 5\%$ in Baryonic Matter

Other contributions to energy (photons, neutrinos,...) are negligible.

Although the numerous successes of the ΛCDM Model, the nature of Dark Energy and Dark Matter is not yet clear. In this thesis, it will be assumed that the Dark Matter is composed of elementary particles, which are only theoretical at the moment, created in the very first instants of life of the Universe. The dispersion velocity of these particles in the formation of structures is negligible, thus we name it Cold Dark Matter.

Over big scales (> 10kpc), the ΛCDM Model has been amply corroborated, and can be considered substantially correct. However, the predictions of the CDM Model diverge significantly from observational data over minor scales (typical of galaxies). It is therefore necessary to develop a new model for the Dark Matter, which replicates the predictions of ΛCDM theory over big scale and concurrently agrees with observational data over minor scales.

An alternative model provides that Dark Matter is "Fuzzy", in the sense that it is composed of extremely light bosons or axions. In particular, the mass of Fuzzy Dark Matter (FDM) particles is expected to be $\approx 10^{-21} - 10^{-22}$ eV otherwise, as shown in the following, FDM wouldn't be able to explain the phenomena for which it is introduced. Thanks to their small mass, these particles have a wave nature that is manifest over astrophysical scales, and that prevents themselves to collapse into the galactic nucleus. Thus, Fuzzy Dark Matter halos are stable for the same reason that makes atoms stable: any attempt to confine a Fuzzy Dark Matter particle under a scale smaller than its huge wavelength would produce an increase in the particle momentum.

More specifically, the so-called "small-scale crisis" is mainly threefold:

- According to cosmological simulations related to the ΛCDM Model, the expected number of dwarf galaxies, which are supposed to populate CDM subhalos, is much larger than the observed one: CDM should form some hundreds of subhalos around the Milky Way, in contrast with the 11 observed dwarf galaxies. This issue goes by the name of *Missing-Satellite Problem*.
- Usually, the baryonic physics is invoked to solve the Missing-Satellite Problem: for example, stellar winds or supernovae could drive the baryonic matter out of small CDM halos. However, these kind of explanations makes another issue to arise: the *Too big to fail problem*, related to the fact that some expected dwarf galaxies are nevertheless too massive to be wiped out.

- It is possible to probe the CDM distribution even near to the galactic cores. However, while numerical simulations describe a singularity in the Dark Matter density for $r = 0$, the value of ρ_{CDM} is observed to be approximately constant in the inner regions of galaxies. This mismatch is the *Cusp-Core Problem*.

In Section 2, the physics that describes FDM particles is presented. The main interest is focused both on the value of their mass, and thus on their De Broglie wavelength, and on the Madelung Equations, a formulation of the Schrödinger equation in terms of hydrodynamics variables. In fact, the superfluid model is much handier to compute numerical simulations with which to compare CDM and FDM models.
Section 3 aims to summarise some of the macroscopic, and therefore observable, features of FDM structures. Moreover, constraints on size, density and mass of Fuzzy Dark Matter halos are derived starting from the properties of FDM particles. Finally, the three main issues of the small-scale crisis are presented in greater detail.
Section 4 is dedicated to the comparison of CDM and FDM density power spectra derived from numerical simulations in the linear regime. In particular, a numerical result derived by Hu, Gruzinov and Barkana ([1]) describing the ratio of the power spectra is initially refined. Then, the same model is studied varying some cosmological parameters (mass of FDM particles, dark matter density and neutrino mass), showing a very weak dependence on these quantities.
Section 5 focuses on the constraints on FDM model provided by the Lyman-alpha forest: after a brief explanation on the nature of the forest and the way it affects the model, a strong constraint on FDM particles mass derived in the nonlinear regime is reported. The number of the Milky Way FDM subhalos is also explicitly calculated according to one of the very few values of m_{FDM} that satisfies the Lyman-alpha forest constraint and approaches to solve the missing-satellite problem. Furthermore, since the constraint imposed by the Lyman-alpha forest clashes with the expected value of m_{FDM}, an attempt to recover the model is presented in the form of mixed models. However, also mixed models are shown to be unable to solve the missing-satellite problem while remaining compatible with the Lyman-alpha forest.
In Section 6 ratios of FDM and CDM power spectra derived with numerical simulations in the nonlinear regime are reported, studied varying redshift and m_{FDM}, and compared with the ones presented in Section 4.
In Appendix A, a more accurate fit for the ratio of FDM and CDM power spectra in the linear regime is derived and analyzed.
In Appendix B, the basic algorithm followed by AX-GADGET (the code used to produce the simulations used in Section 6) is illustrated.

2 The Physics of Fuzzy Dark Matter

Fuzzy Dark Matter is composed of extremely light particles. However, the presence of some particles with small or zero mass is a characteristic common to many field theories, therefore it is not necessary to introduce these particles to specially justify the FDM ([2]). The reason that makes these particles so widespread concerns their extra symmetry (exact or approximate), evident in the action

$$I = \frac{1}{2}\int d^4x\sqrt{-g}g^{\mu\nu}\partial_\mu\phi\partial_\nu\phi \tag{1}$$

which is symmetric for the shift transformation $\phi \to \phi + C$, where C is a constant. This symmetry is obviously lost if a mass term or a coupling (self coupling or with other fields) is introduced. If we introduce a very small mass or coupling, the exact symmetry is downgraded to an approximate one.

A remarkable example of an approximate shift symmetry can be found in the action of the "axionlike fields", that is characterized by two parameters F and a

$$I = \int d^4x\sqrt{-g}\left[\frac{1}{2}F^2g^{\mu\nu}\partial_\mu a\partial_\nu a - \mu^4(1-\cos a)\right] \tag{2}$$

This action is clearly symmetric under the shift transformation $a \to a + 2\pi$, where a is a dimensionless scalar field. The mass of axions can be obtained by expanding the term in the round parenthesis at the first order in a and dividing by F^2, so to obtain

$$I = \int d^4x\sqrt{-g}F^2\left[\frac{1}{2}g^{\mu\nu}\partial_\mu a\partial_\nu a - \frac{\mu^4}{F^2}a^2\right] \tag{3}$$

It is easy to identify the mass term for a

$$m_a = \frac{\mu^2}{F} \tag{4}$$

In particular, it is possible to obtain $m_a \sim 10^{-21} - 10^{-22}\,\text{eV}$ for appropriate μ and F; therefore these fields are good candidates for FDM. The exact value of F varies according to the model, but in most cases it lies between the GUT scale $10^{16}\,\text{GeV}$ and the reduced Planck mass $10^{18}\,\text{GeV}$ ([2]).

$$10^{16}\,\text{GeV} \lesssim F \lesssim 10^{18}\,\text{GeV} \tag{5}$$

Also μ depends on the model, but it can be roughly valued by

$$\mu^4 \approx M_{Pl}^2\Lambda^2e^{-S} \tag{6}$$

where S is the instanton[1] action and Λ is an estimation of the suppression of instanton effects due to supersimmetry, and covers a very wide spectrum of values:

[1] An instanton is a solution to the equations of motion of the classical Field Theory on a Euclidean spacetime.

$$10^4\,\mathrm{GeV} \lesssim \Lambda \lesssim 10^{18}\,\mathrm{GeV} \tag{7}$$

However, Λ typical values are $10^{18}\,\mathrm{GeV}$, $10^{11}\,\mathrm{GeV}$ and $10^4\,\mathrm{GeV}$, depending on how (and if) the suppression occurs. Taking $F \approx 10^{17}\,\mathrm{GeV}$ - an indicative value of the previously calculated range - it is possible to calculate the value of S that produces $m_a = 10^{-22}\,\mathrm{eV}$.

$$S = \begin{cases} 165, & \text{if } \Lambda \text{ is } 10^4\,\mathrm{GeV} \\ 198, & \text{if } \Lambda \text{ is } 10^{11}\,\mathrm{GeV} \\ 230, & \text{if } \Lambda \text{ is } 10^{18}\,\mathrm{GeV} \end{cases} \tag{8}$$

which are reasonable values for S, as can be shown considering the very rough formula[2] $S \approx 2\pi/\alpha_G$, where α_G is the Standard Model coupling constant at GUT energy. Taking $\alpha_G = 1/25$, it follows that $S \approx 157$, which is of the same order magnitude of the previously calculated S, so there is another reason to expect $m_a \approx 10^{-22}\,\mathrm{eV}$.

It is also possible to estimate F analyzing the evolution of the axionlike field a. The first thing to notice is the impossibility to know the value taken by the axionlike field in the very early Universe. In fact, as the axionlike field potential in (2) is $\mu^4(1-\cos a)$, it would have been written more generally as $\mu^4(1-\cos(a-a_0)$, where we have assumed $a_0 = 0$. Indeed, the value of a_0 depends on the mechanism that breaks the shift symmetry when the energy of the field drops down. However, whatever mechanism determines the value of a in the early Universe do not permit us to find out what is the value of a that minimizes the potential at low energies. For this reason, the only possible choice is to take the initial value of a as random. Furthermore, a is intended to remain constantly equal to its initial random value as long as $H \gtrsim m_a$. This is a consequence of the equation of motion of an oscillating field that depends only on time in a Friedmann-Robertson-Walker Universe:

$$\ddot{a} + 3H\dot{a} + m_a^2 \sin a = 0 \tag{9}$$

It is straightforward to notice that, for $H \gg m_a$, the value of a is constant (since equation (9) is solved for $\dot{a} = 0$). When this condition is no longer valid, a starts oscillating with angular frequency $m_a c^2/\hbar$ (once restored $\hbar$ and c), and the amplitude of the oscillations is damped as $R^{-\frac{3}{2}}$. Moreover, the energy of this field scales as R^{-3}, so it is consistent with the behavior of Cold Dark Matter.

When $H \sim m_a$, the temperature has reached the value T_0, that satisfies the rough relation

$$\frac{T_0^2}{M_{Pl}} = m_a \tag{10}$$

Furthermore, the energy density of radiation is T_0^4, while the Dark Matter one is approximately μ^4 (from equation (2)). Remembering that

[2]This formula is valid only in a few simple cases, but can still be used to find out what values of S are reasonable.

$$\frac{\rho_a}{\rho_\gamma} \propto \frac{1}{T} \tag{11}$$

where ρ is referred to the energy density of Dark Matter and radiation, it is clear that they are equal when $T \approx T_1 \approx 1\,\mathrm{eV}$. Briefly, it is possible to refer to the following rough relation:

$$\frac{\mu^4}{T_0^4}\frac{T_0}{T_1} \sim 1 \tag{12}$$

And recalling the relation between μ, F and m_a

$$\mu^4 = F^2 m_a^2 \tag{13}$$

It is possible to obtain the value of F that is in agreement with the fact that the field a is a candidate for Dark Matter:

$$F \sim \frac{M_{Pl}^{\frac{3}{4}} T_1^{\frac{1}{2}}}{m_a^{\frac{1}{4}}}\Big|_{m_a = 10^{-22}\,\mathrm{eV}} \sim 0.5 \cdot 10^{17}\,\mathrm{GeV} \tag{14}$$

It's interesting to notice that two separate arguments about Fuzzy Dark Matter have led to the same value of F (and, consequently, of μ).

An estimation of T_0 allows to understand when the axionlike field begins to oscillate:

$$T_0 \sim \sqrt{m_a M_{Pl}} \sim 500\,\mathrm{eV} \tag{15}$$

that corresponds to a redshift of $\sim 2 \cdot 10^6$. So, FDM begins to oscillate after nucleosynthesis (which happens at redshift $\sim 3 \cdot 10^8$). For this reason, and recalling that the energy density of a is approximately constant before it starts to oscillate, it is possible to conclude that FDM acts as a form of Dark Energy (distinguished precisely by having ρ constant) during nucleosynthesis. However, the contribution of FDM to Dark Energy is negligible ([2]).

Another issue concerns axion self-interaction. Until now, the dynamics of the FDM field have been considered as purely gravitational, but it's easy to notice that action (2) generates also a self-interaction term in the equation of motion:

$$D^\mu D_\mu a + m_a^2 a - \frac{m_a^2}{6} a^3 + \mathcal{O}(a^5) = 0 \tag{16}$$

In what limits the (attractive) self-interaction term $\frac{m_a^2}{6}a^3$ can be neglected? To answer, we have to compare $m_a^2 a^3$, which represents the self-interaction - with the gravitational term $\epsilon m_a^2 a$, where ϵ is the gravitational potential. So, we have to figure out if $m_a^2 a^3 \gtrsim \epsilon m_a^2 a \rightarrow a^2 \gtrsim \epsilon$.

For $T = T_0$ - when the field begins to oscillate - a still has its initial random value, so we have $a^2 \approx 1$. At the same time, ϵ has the value of the primordial cosmic fluctuations: $\epsilon \sim 10^{-5}$. Therefore, in the early Universe, $a^2 \gg \epsilon$ and the self-interaction term

dominates. Things change as the Universe ages. Since $a \sim R^{-\frac{3}{2}}$, the gravitational term begins to dominate when R increases by a factor of about $10^{\frac{5}{3}}$, i.e. when $a^2 \approx \epsilon$. In other terms, gravity dominates when the temperature is dropped below $T_0 \cdot 10^{-\frac{5}{3}}$. It is important to notice that gravity is already dominating the FDM dynamics when the radiation-matter equality is reached.

There is often another type of potential in dealing with FDM: $\epsilon \sim G\rho L^2$, which represents the gravitational potential generated by a weakly bound object with density ρ and size L. In this case, the dynamics are dominated by gravity if $a^2 \gtrsim \epsilon \sim G\rho L^2$. Remembering that, for an axionlike field, $\rho \sim F^2 m_a^2 a^2$, it is easy to obtain $1 \gtrsim GL^2F^2m_a^2$, and substituting $G = \frac{1}{8\pi M_{Pl}^2}$ it is possible to conclude that the self-interaction term dominates the dynamics of this object if

$$L \lesssim \frac{\sqrt{8\pi}M_{Pl}}{Fm_a} \sim 1\,\mathrm{pc} \tag{17}$$

Considering that FDM particles have a De Broglie wavelength of ~ 1 kpc, we will always neglect self-interaction term for FDM candidates.

Another question concerns the actual possibility of detecting FDM particles. In fact, due to their extremely small mass and weak coupling with ordinary matter, any conventional search for Fuzzy Dark Matter candidates would not be successful. However, some proposal for direct observation of axionlike particles have been made by Arvanitaki et al. ([3]).

In particular, axionlike candidates for FDM with mass included in the range $10^{-22}\,\mathrm{eV} \lesssim m_a \lesssim 10^{-10}\,\mathrm{eV}$ can affect the dynamics and gravitational wave emission of rapidly rotating black holes by the Penrose superradiance process: an effect resulting from the entry of matter in the ergoregion of a Kerr Black Hole. Once entered in the ergoregion, the matter is split in two parts: one could fall into the event horizon, while the other could exit the ergoregion. The emitted matter has in general more energy than the entire matter that initially entered the ergoregion. The energetic imbalance of the emitted matter is at the expense of the rotational energy of the black hole, which loses some of its angular momentum. This loss of angular momentum affects the gravitational waves emitted by the black hole, through which the decrease of energy of the black hole could be detected. The value $m_a \approx 10^{-22}\,\mathrm{eV}$ is not optimal for this technique, but can still be detected.

Other possibilities to detect FDM candidates involve CASPEr axion experiment ([4]) and, less directly, the observations of pulsar timing ([5]).

2.1 The Superfluid Model for Fuzzy Dark Matter

As shown previously, in studying FDM it is possible to ignore its self-interaction. Thus FDM candidates action is

$$S = \int \frac{d^4x}{\hbar c^2}\sqrt{-g}\left[\frac{1}{2}g^{\mu\nu}\partial_\mu\phi\partial_\nu\phi - \frac{1}{2}\frac{m^2c^2}{\hbar^2}\phi^2\right] \tag{18}$$

which describes the motion of a scalar ϕ (related to the axionlike field a by the relation $\phi = Fa$) minimally coupled to the metric $g^{\mu\nu}$. Instead of studying the field ϕ directly, in the nonrelativistic limit it is convenient to express ϕ in terms of another scalar field ψ, whose equation of motion is derived.

$$\phi = \sqrt{\frac{\hbar^3 c}{2m}} \left(\psi e^{\frac{-imc^2 t}{\hbar}} + \psi^* e^{\frac{imc^2 t}{\hbar}} \right) \tag{19}$$

The equation of motion of ψ has the form of a slightly modified Schrödinger equation ([6])

$$i\hbar \left(\dot{\psi} + \frac{3}{2} H\psi \right) = \left(-\frac{\hbar^2}{2mR^2} \nabla^2 + m\Phi)\psi \right) \tag{20}$$

where the $\ddot{\psi}$ term is neglected and a FRW metric perturbed by the gravitational potential $\Phi(\mathbf{r}, t)$ is adopted:

$$ds^2 = \left(1 + \frac{2\Phi}{c^2} \right) c^2 dt^2 - R^2(t) \left(1 - \frac{2\Phi}{c^2} d\mathbf{r}^2 \right) \tag{21}$$

where $R(t)$ is the scale factor.

It is now convenient to consider Dark Matter as a superfluid, so it is necessary to define its fluid density ρ and velocity $\mathbf{v}$:

$$\begin{cases} \psi \equiv \sqrt{\frac{\rho}{m}} e^{i\theta} \\ \mathbf{v} \equiv \frac{\hbar}{Rm} \nabla\theta = \frac{\hbar}{2miR} \left(\frac{1}{\psi} \nabla\psi - \frac{1}{\psi^*} \nabla\psi^* \right) \end{cases} \tag{22}$$

Applying these definitions to the ψ equation of motion in comoving coordinates, one obtains the following relations:

$$\begin{aligned} \dot{\rho} + 3H\rho + \frac{1}{R} \nabla \cdot (\rho \mathbf{v}) = 0 \\ \dot{\mathbf{v}} + H\mathbf{v} + \frac{1}{R} (\mathbf{v} \cdot \nabla)\mathbf{v} = -\frac{1}{R} \nabla\Phi + \frac{\hbar^2}{2R^3 m^2} \nabla \left(\frac{\nabla^2 \sqrt{\rho}}{\sqrt{\rho}} \right) \end{aligned} \tag{23}$$

These are the Madelung equations ([6]) and the modified Navier-Stokes equation, adjusted with terms proportional to H to take in account the expansion of the Universe. The Madelung equations are essentially an alternative formulation of the Schrödinger equation, written in terms of hydrodynamics variables. They can be considered a quantum generalization of the Navier-Stokes equation for fluid dynamics (which are derived, in turn, by application of the Newton's Second Law to fluid motion). Besides the terms that describes the expanding Universe contribute, the difference between Madelung and Navier-Stokes equations is contained in the term $\frac{\hbar^2}{2R^3 m^2} \nabla \left(\frac{\nabla^2 \sqrt{\rho}}{\sqrt{\rho}} \right)$, which is commonly referred to as the "quantum pressure" term. This contribute causes the fluid to acquire a certain rigidity against compression.

The advantage in using the Madelung equations instead of Schrödinger one concerns the fact that the superfluid model is simpler to treat with numerical simulations, which are the main means to compare FDM and "standard" Dark Matter models.

3 FDM constraints and predictions over small scales

As said in Section 1, predictions of CDM and FDM models over scales bigger than $\sim$ 10kpc, where they reproduce correctly the observational data. However, the two models differ over smaller scales. In particular, none of CDM predictions have been observed in the Milky Way or other Local Group galaxies, while it will be shown that FDM models are more successful in describing the same astrophysical data. In the following, some of the numerous comparisons between FDM predictions and observational data are described.

3.1 Limits on size and density of a FDM structure

A first constraint on FDM emerges studying the equilibrium of a self-gravitating system. The confrontation between the kinetic and potential energy of such a system brings to the definition of its virial radius, that is associated with stability. If the de Broglie wavelength of FDM candidates were bigger than the virial radius, the system could not reach the stability. This fact establishes a lower limit to the size of FDM structures:

$$\frac{\lambda}{2\pi} \leq r_{vir} \approx \frac{GM}{v^2} \rightarrow r \geq \frac{\hbar^2}{GMm^2} \tag{24}$$

A more precise reasoning brings to a lower limit for $r_{1/2}$: the radius containing half of the mass of a spherically symmetric, time-independent, self-gravitating system of FDM ([2]).

$$r_{1/2} \geq 3.925 \frac{\hbar^2}{GMm^2} \tag{25}$$

Inserting data ($M = 10^9 M_\odot, m = 10^{-22}\,\mathrm{eV}$) in equation (25), one obtains 0.335kpc as lower limit for $r_{1/2}$. The equality is reached if the system is the state that minimizes the energy, which is called "soliton". This constraint reveals a strange property of self-gravitating time independent FDM systems supported by quantum pressure: the larger is the mass of the structure the smaller is its scale.

Developing (25) it is possible to derive an upper limit for the central density of an FDM structure.

$$\rho_c = \frac{M}{\left(\frac{4\pi r_{1/2}^3}{3}\right)} \leq 0.0044 \left(\frac{Gm^2}{\hbar^2}\right)^3 M^4 \tag{26}$$

Again, inserting data in this equation one obtains an upper limit of $7.05 M_\odot \mathrm{pc}^{-3}$ for the central density of an FDM structure (i.e. an upper limit on the density inside a sphere of radius $r_{1/2}$). This limit offers the possibility to test the FDM model by comparison with observational data. More precisely, it is possible to compare this result with the observed central densities of dwarf spheroidal galaxies in the Local Group. These galaxies are, in fact, strongly dominated by dark matter, and then represent the

most severe test for the model. However, the maximum value of the central density of a dwarf galaxy observed in the Local Group is $5M_{\odot}\mathrm{pc}^{-3}$, which is consistent with the FDM model ($m_{FDM} = 10^{-22}\,\mathrm{eV}$ and $M_{halo} \approx 10^{8} - 10^{9}M_{\odot}$).

Therefore, it is possible to extract another remarkably confirm of the FDM model by analyzing the dwarf spheroidal galaxies. If we assume that the central part of these galaxies is a soliton, it is possible to obtain a reasonable value for the FDM particles mass by studying the kinematics of the stars orbiting around it. Using this approach, two estimates for the FDM candidate mass were obtained ([7]):

- $m = 8^{+5}_{-3}10^{-23}\,\mathrm{eV}$
- $m = 6^{+7}_{-2}10^{-22}\,\mathrm{eV}$

These measures are compatible both with each other and with the assumptions of the FDM model.

3.2 Effects due to the relaxation in systems composed of FDM

FDM is successful in describing several phenomena which are inconsistent with the standard CDM models (in particular the cusp-core and the missing-satellite problems). Most of these matters deal with the relaxation[3] in systems composed of FDM. In the following, relaxation for FDM is firstly described, and below some of the problems are presented and faced using the FDM model.

3.2.1 Relaxation in FDM systems

Due to the fact that FDM and standard CDM follow the same behavior over big scales, it is reasonable to expect that the soliton is surrounded by a Dark Matter virialized halo, which density follows a Navarro-Frenk-White profile ([8]):

$$\rho_{NFW}(r) = \frac{\rho_0}{\frac{r}{R_s}\left(1+\frac{r}{R_s}\right)^2} \tag{27}$$

where ρ_0 and R_s are parameters that describe the central density and the "scale radius" of any particular halo. This conclusion is confirmed by simulations ([9]).

[3]Relaxation is the process that drives a perturbed system to the equilibrium, and is characterized by a relaxation time.

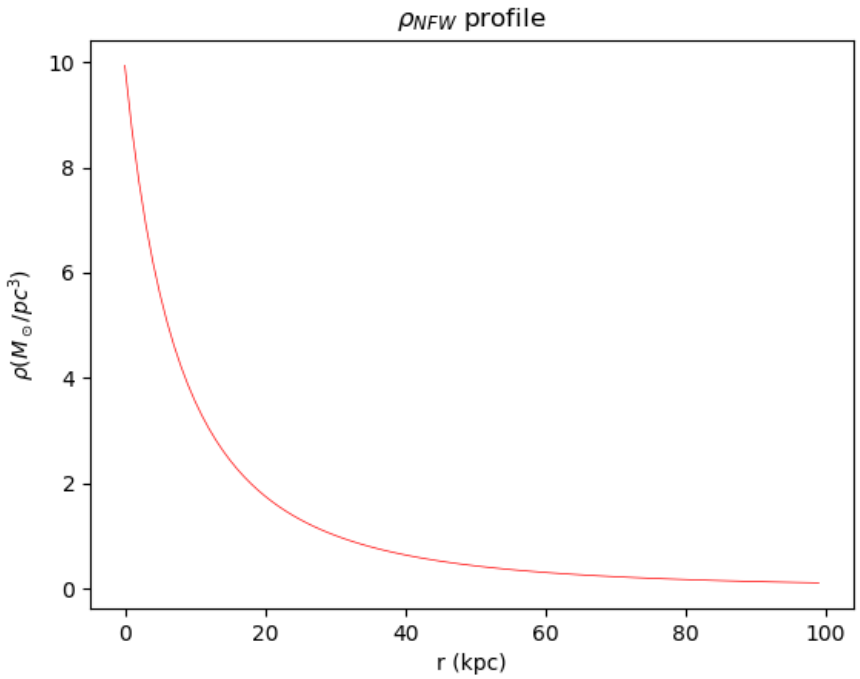

Figure 1: Navarro-Frenk-White profile that describes the density of the halo surrounding a soliton with $\rho_0 = 5M_\odot/\text{pc}^3$ and $R_s = 0.335\text{kpc}$

It is also possible to use the simulations to derive a relation between the masses of the soliton and the surrounding halo:

$$M_{soliton} \approx 2.7 \cdot 10^8 M_\odot \frac{10^{-22}\,\text{eV}}{m} \left(\frac{M_{halo}}{10^{10} M_\odot}\right)^{1/3} \tag{28}$$

Despite the fact that most of the mass is in the halo, these simulations show that there is a two order of magnitude gap between the FDM density in the halo and in the soliton. Moreover, increasing the mass of the halo, one occurs in two surprising consequences: the gap between the halo and soliton densities grows up, and the soliton mass becomes even smaller than the one estimated by using equation (28). To understand this last fact, it is necessary to investigate on the relaxation process that occurs in a FDM system.

First, an isolated CDM system in equilibrium (i.e., composed of non collisional Dark Matter particles) evolves only through two-body relaxation ([10]). It is also possible to derive an expression for the characteristic time of the process:

$$t_{relax} \approx 0.1 \frac{rM}{vm} \tag{29}$$

Substituting typical values for M and m, one finds that the relaxation time is in general much bigger than the Hubble time, so the process can be neglected.

Things are different if the system is composed of FDM instead of standard CDM. In this case, every eigenstate different from the soliton is unstable, and the whole system is destined to collapse into a soliton by a process called "Gravitational Cooling". Moreover, the wavy granularity, which is the source of the relaxation process for FDM systems, is due to two phenomena ([2]):

- The finite number of eigenstates in the halo (of order $\left(\frac{2\pi r}{\lambda}\right)^3$)
- The spatial correlation in density fluctuations that arises because the FDM particles are bosons.

It is possible to roughly estimate the relaxation time given by the density fluctuations. Let ρ be the local density of an FDM halo. As a consequence, FDM acts as quasiparticles, with effective mass $m_{eff} \sim \rho(\lambda/2)^3$. Again, a rough estimation of the relaxation time is given by the formula (29), where we substitute the effective FDM mass in place of m and write $M \sim \frac{4}{3}\pi\rho r^3$, the halo mass included in a sphere with radius r.

$$t_{relax}(r) \sim \frac{rM}{vm_{eff}} \sim \frac{0.4}{f_{relax}} \frac{m^3 v^2 r^4}{\pi^3 \hbar^3} \tag{30}$$

Where $f_{relax} \lesssim 1$ is a dimensionless constant. Finally, we find that the relaxation time for an FDM system composed of an FDM quasiparticle with mass 10^{-22} eV, orbiting around a sphere of radius 5kpc at a velocity of 100 Km/s is about $\frac{10^{10}}{f_{relax}}$ years.

Briefly, every FDM halo will slowly develop a solitonic core with the mass included in a radius r_s, where r_s satisfies the relation $t_{relax}(r_s) = t_0$ (and t_0 is the age of the halo). An important fact to notice is the relation between the relaxation time and the velocity and radius of the halo. Low-mass halos have also small radius and velocity, so their relaxation time will be very short if compared with higher-mass halos. Consequently, most of the mass of the small halos is collapsed in the soliton by gravitational cooling, and as the mass grows the relaxation time becomes bigger. Thus, as anticipated, in big halos only a small fraction of the mass is collapsed in the soliton.

The fluctuating potential has effects on some structures that populates the galaxy. In the following, some of these will be analyzed, so it is important to estimate the physical quantities that are going to be used. As a rough estimate is sufficient, we can examine the Milky Way at the distance of the Sun. Therefore, we have: $r \sim 10$kpc, $v \sim 200$ Km/s and $\rho \sim 0.01 M_\odot pc^{-3}$. Assuming that FDM particles have a mass of 10^{-22} eV, we can calculate the de Broglie wavelength $\lambda \sim 600$pc, and lastly the mass of a typical FDM quasiparticle $m_{eff} \sim \rho(\lambda/2)^3 \sim 3 \cdot 10^5 M_\odot$.

3.2.2 Disruption of star clusters and wide binary stars

The fluctuating potential generated by FDM exerts tidal forces on bounded structures, such as star clusters and binary stars. In some cases, the tidal forces are strong enough to disrupt these structures. Now we are going to determine if the characteristic time

of the process is short enough to make it physically interesting. An estimation of the disruption time for star clusters is given by the equation ([11])

$$t_{dis} \simeq \frac{0.05}{f_{relax}} \frac{\sigma_v m_{cl} r_h^2}{G m_{eff} \rho a^3} \tag{31}$$

Where $\sigma_v \sim v$ is the dispersion in relative velocity, m_{cl} is the mass of the cluster, $r_h \sim \lambda/2$ is the half-mass radius of the perturber and a is the semimajor axis of the cluster star. Inserting the following parameters (suitable for a globular cluster)

v	m_{cl}	m	ρ	a
$200\,\mathrm{Km/s}$	$3 \cdot 10^5 M_\odot$	$10^{-22}\,\mathrm{eV}$	$0.01 M_\odot \mathrm{pc}^{-3}$	$30\mathrm{pc}$

one obtains that $t_{dis} = \frac{8.4 \cdot 10^{11}\mathrm{yr}}{f_{relax}}$ Thus, the disruption time seems to have no physical interest. However, it is possible that some globular clusters orbit very near to the Galactic core, in which the FDM density is much larger. Thanks to the relation $t_{dis} \propto \rho^{-2}$ and assuming $f_{relax} \approx 1$, it is reasonable to expect that the tidal forces produce observable effects on the globular clusters that are very close to the Galactic core, like the shear of their outer parts.

Nevertheless, FDM fluctuating potential cannot affect considerably the open clusters. In fact, in this case nominal values are

v	m_{cl}	m	ρ	a
$200\,\mathrm{Km/s}$	$300 \cdot 10^5 M_\odot$	$10^{-22}\,\mathrm{eV}$	$0.01 M_\odot \mathrm{pc}^{-3}$	$2\mathrm{pc}$

So one finds $t_{dis} \approx 2 \cdot 10^{11}/f_{relax}\mathrm{yr}$, much longer than the typical age of $3 \cdot 10^8\mathrm{yr}$ of open clusters themselves.

The same mechanism might disrupt a system of binary stars. We can use equation (31) and replace m_{cl} with the mass of the binary system $m_{bin} \sim 2M_\odot$. The widest binary stars have $a \sim 0.1\mathrm{pc}$. With these data one obtains $t_{dis} \sim \frac{1.5 \cdot 10^{14}\mathrm{yr}}{f_{relax}}$, again a time much longer than the typical age of stars.

3.2.3 Effects of FDM on the orbits of merging black holes

Supermassive black holes ($10^6 - 10^{19} M_\odot$) are usually in the center of a galaxy. Then, the merger of two black holes of this kind is supposed to occur when two galaxies collide. In particular, the process that leads the two black holes to spiral and eventually merge is influenced by the presence and kind of Dark Matter. This is an important fact, because the last stages of the inspiral are characterized by the emission of a large amount of energy in the form of gravitational waves, that could be detected and studied.

However, FDM density fluctuations could hinder the inspiral at kiloparsec scales. This occurs when the mass of the fluctuations is even larger than that of the black holes, because in this case the fluctuations pump energy into the black hole system and compensate its loss due to dynamical friction. Thus, the effect of FDM quasiparticles on merging black holes is similar to the disruption of binary star systems.

It is possible to estimate the scale at which the FDM can prevent the collapse of the two black holes. The effective mass of FDM quasiparticles is about $m_{eff} \sim \rho\frac{\lambda^3}{8}$, and a nominal value for ρ (the mean density inside radius r) can be obtained by supposing that the mean density is dominated by the FDM density ρ_{FDM}. Under this assumption, one obtains:

$$m_{eff}\frac{v^2}{r} = G\frac{m_{eff}^2}{r^2} \rightarrow \rho_{FDM} = \frac{3m_{eff}}{4\pi r^3} = \frac{3v^2}{4\pi G r^2} \tag{32}$$

And remembering that $\lambda = \frac{2\pi\hbar v}{m}$, we conclude that

$$m_{eff} \sim \frac{3\pi^2\hbar^3}{4Gr^2m^3v} = 6\cdot 10^7 M_\odot \left(\frac{1\text{kpc}}{r}\right)^2 \left(\frac{200\,\text{Km/s}}{v}\right)\left(\frac{10^{-22}\,\text{eV}}{m}\right)^3 \tag{33}$$

Thus, the merge of smaller black holes can be hindered by FDM density fluctuations at the scale of 1kpc. More precisely, the orbital decay may be stopped and even reversed if $\rho_{FDM}m_{eff} \gtrsim \rho_* m_{BH}$, where ρ_* is the non-rotating stellar system. In this case, the formation of subparsec black holes binaries would be suppressed. This would be a remarkable success of the FDM model, but unfortunately the predicted population of supermassive black holes orbiting at kiloparsec distances from the center of galaxies would be extremely difficult to detect.

3.2.4 FDM solitonic disk

Since the relaxation time computed in equation (29) and (30) is smaller than the typical age of a halo, it is possible that an FDM disk is formed around the soliton. Such a disk could be characterized using three variables:

- The density $\rho_{FDM}(r)$, which should be symmetric around $r = 0$ and indeed can be described by its value at this point: $\rho_{FMD}(r = 0)$.
- The surface density $\Sigma_{FDM} = \int_{-\infty}^{\infty} \rho_{FDM}(r)dr$.
- The half-thickness $r_{1/2}$, defined as the distance within which half of the mass is enclosed: $\int_0^{r_{1/2}} \rho_{FDM}(r) = \frac{1}{2}\int_0^{\infty} \rho_{FDM}(r)$.

These features may be estimated by computing the ground state of the Schrödinger-Poisson equation in one dimension (because of the symmetry of ρ_{FDM}, r is the only interesting variable), while *assuming that the baryonic contribution to the gravitational potential is neglectable*. In particular, assuming that $\Sigma_{FDM} \sim 100 M_\odot \text{pc}^{-2}$, $\rho_{FDM}(0)$ and $r_{1/2}$ are given by ([2]):

$$\begin{aligned} \rho_{FDM}(0) &= 0.984\left(\frac{G\Sigma_{FDM}^4 m^2}{\hbar^2}\right)^{1/3} = 0.104 M_\odot \text{pc}^{-3} \\ r_{1/2} &= 0.2744\left(\frac{\hbar^2}{G\Sigma_{FDM}m^2}\right)^{1/3} = 260\text{pc} \end{aligned} \tag{34}$$

However, the total density in the Galactic midplane is $\rho(0) = 0.10 \pm 0.01 M_\odot \mathrm{pc}^{-3}$, and it is strongly affected by the baryons. In particular, for $m_{FDM} = 10^{-22}$ eV, the maximum value of the surface density of the FDM disk in the solar neighborhood is $20 M_\odot \mathrm{pc}^{-2}$. Therefore, since the new value of the central density is $\rho_{FDM}(0) \lesssim 0.012 M_\odot \mathrm{pc}^{-3}$, the assumption that the baryonic contribution is neglectable is inconsistent. On the contrary, one could try to calculate $\rho_{FDM}(0)$ and $r_{1/2}$ starting from the assumption that the gravitational potential is dominated by the baryons. The new values are given by ([2]):

$$\begin{aligned} \rho_{FDM}(0) = 1.141 \frac{\Sigma_{FDM}}{\Sigma_b} \left(\frac{G \Sigma_b^4 m^2}{\hbar^2} \right)^{1/3} &= 0.120 M_\odot \mathrm{pc}^{-3} \\ r_{1/2} = 0.2399 \left(\frac{\hbar^2}{G \Sigma_b m^2} \right)^{1/3} &= 228 \mathrm{pc} \end{aligned} \tag{35}$$

where $\Sigma_b \sim 51 M_\odot \mathrm{pc}^{-2}$ is the baryons surface density along an approximated zero-thickness sheet that underlies the FDM disk. Taking $\Sigma_{FDM} \sim 17 M_\odot \mathrm{pc}^{-2}$, one arrives to $\rho_{FDM}(0) = 0.016 M_\odot \mathrm{pc}^{-3}$ and to $r_{1/2} = 285$pc. Therefore, although an FDM disk would have a thickness comparable to the baryonic matter one, it would only make a small contribution ($\sim 20\%$) to the total density in the solar neighborhood. This result is strongly affected by the value of m_{FDM}. In fact, assuming it equal to 10^{-21} eV, the FDM central density would be comparable to the baryonic one and the disk would be thinner than the stellar one.

3.3 Lower bound on FDM halo masses

FDM halos significantly less massive than $10^7 M_\odot$ cannot exist. This fact arises from two separate arguments that produce the same result. One limit comes from the fact that every structure formed by gravitational collapse, like Dark Matter halos, cannot be less dense than the average Universe. Thus, we firstly define the mean density contained in the half-mass radius $\rho_{1/2} \equiv \frac{1}{2} \frac{M}{\frac{4}{3} \pi r_{1/2}^3}$. It has to be compared with $\rho_{vir} \approx 200 \rho_c$, the density that defines the virial radius in terms of the critical density $\rho_c = \frac{3H^2}{8\pi G}$. More precisely, we are requiring that $\rho_{1/2} > q \rho_{vir}$, where $q \gtrsim 1$ is a factor introduced to account for the roughness of the estimate. Following this approach we get to

$$M > 1.4 \cdot 10^7 M_\odot q^{\frac{1}{4}} \tag{36}$$

The second argument is based on the Jeans length: the minimal radius that a density fluctuation needs to have to collapse. In particular, the Jeans analysis for FDM produces the critical wave number ([2])

$$k_J = \frac{2 (\pi G \rho)^{\frac{1}{4}} m^{\frac{1}{2}}}{\hbar^{\frac{1}{2}}} \tag{37}$$

where ρ is the background matter density. It is possible to derive the corresponding Jeans wavelength $\lambda_J \equiv \frac{2\pi}{k_J}$, and finally the Jeans mass

$$M_J = \frac{4}{3}\pi\rho\left(\frac{1}{2}\lambda_J\right)^3 = 1.5\cdot 10^7 M_\odot (1+z)^{\frac{3}{4}}\left(\frac{\Omega_{FDM}}{0.27}\right)^{\frac{1}{4}}\left(\frac{H_0}{70\,\mathrm{Km/sMpc^{-1}}}\right)^{\frac{1}{2}}\left(\frac{10^{22}\,\mathrm{eV}}{m}\right)^{\frac{3}{2}} \tag{38}$$

where Ω_{FDM} is the fraction of FDM density over the critical one.

Thus, two independent arguments bring to the same lower limit $M > (1.4 - 1.5)\cdot 10^7 M_\odot$ for FDM halo masses. This constitutes an opportunity for comparison between FDM and CDM models. In fact, the last provides that the number of halos less massive than $10^8 M_\odot$ drops down very quickly as $n(M_h) \propto M_h^{-1}$ ([12]), so the presence of a large number of low-mass halos would weaken the CDM models and favor FDM.

3.4 The cusp-core problem

One of the most discussed issues about the small scale crisis of Cold Dark Matter is the so-called cusp-core problem, that arises analyzing the rotation velocity of objects in the inner part of galaxies. Obviously, stars populate these regions, and they are certainly the cause of a fraction of the rotation velocities. Therefore, it is important to take into account that the motion of objects near the galactic nucleus is strongly affected by baryionic matter, while the rotational velocity outside the galaxy is dominated by dark matter. It is however possible to trace the dependence of the rotational velocity on dark matter density even in the inner part of the galaxies, where velocities are found to rise approximately linearly with the radius ([13]). This observation is consistent with the presence of a central core in the dark matter distribution. However, the first results of numerical N-body simulations of dark matter halos based on collisionless CDM were not consistent with the core-distribution, showing rather that the rotation curves rise as the square root of the radius and that dark matter density decreases as $\rho \sim r^{-1}$ ([14]). Therefore, numerical simulations describes a steep power-law density distribution, i.e. a cusp. One of the first models describing the steep power law trend of dark matter density was proposed by Navarro, Frenk and White in 1997, and has already been reported in Figure 1. It has been argued that baryonic processes might be the cause of the observed core distribution. For example, Navarro et al. ([15]) used N-body simulations to model the effect of star formation on the baryons and the dark matter, and found that a central dark matter core can be created if a large fraction of the baryons is suddenly expelled into the halo.

However, Burkert ([16]) analyzed four dwarf galaxies and came to the conclusion that their rotation curves, after appropriate scaling, are self-similar. Therefore, it is unlikely that baryonic physics blow-outs and mass-flows can accurately explain the presence of cores, and attributed the linear rise of the rotation curves to the intrinsic properties of dark matter. Moreover, Burkert found evidence that the mass density in the outer parts of these four dwarf galaxies drops off as r^{-3}, i.e. consistent with dark matter, and not as r^{-2}, as suggested by the rotation curves of spiral galaxies. Finally, he proposed the so-called "Burkert profile" to describe this behavior:

$$\rho(r) = \frac{\rho_0 r_0^3}{(r + r_0)(r^2 + r_0^2)} \tag{39}$$

where ρ_0 and r_0 are respectively the core density and radius. This model reproduces the trend of rho both for r both small ($\rho \sim$ const) and big ($\rho \sim r^{-3}$).

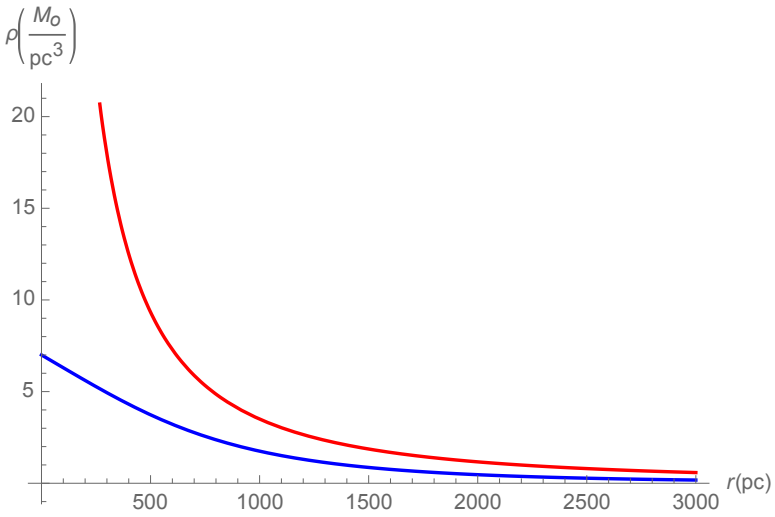

Figure 2: Navarro-Frenk-White profile, in red, displays a cusp for $r \sim 0$, while Burkert profile, in blue, remains finite for $r \sim 0$. In both profiles, $r_0 = R_s = 1000$ pc, which has been shown to be a rough estimate of the soliton radius, and $\rho_0 = 7 M_\odot/\text{Mpc}^3$, the upper limit of the density of an FDM structure. (Plot computed with Wolfram Mathematica [17])

One of the main differences between the predictions of FDM and CDM models regards the Dark Matter density in the center of halos. Indeed, CDM models predict that the density in Dark Matter halos goes roughly as $\rho \sim r^{-1}$, so there would be a cusp for $r \approx 0$. On the contrary, as said in Section 2, FDM halos envelope a soliton core at their center, and therefore is consistent with the presence of cusps in the center of dark matter halos. Currently, the problem has not been solved. In particular, the dwarf spheroidal galaxies are being studied because their density is strongly dominated by Dark Matter, so it would be easier to reveal a cusp or a core in the Dark Matter distribution ([18]). However, although the observations of stellar kinematics are more consistent with the presence of cores predicted by FDM model than with the cusps, a final answer has not been reached yet.

3.5 The missing-satellite problem

The missing-satellite problem arises from numerical cosmological simulations that predict the evolution of the distribution of matter in the Universe. In particular, Dark Matter seems to cluster hierarchically, i.e. every halo is surrounded by others smaller

subhalos. Further, the number of subhalos increases as the iteration proceeds. However, whilst the number of normal-sized galaxies, corresponding to normal-sized halos, is in agreement with the predicted result, the number of dwarf galaxies observed in the Milky way, i.e. of small-sized halos, is far less than the expected.
For comparison, simulations suggest that the Milky Way has up to 500 dwarf satellite galaxies (depending on the model), while only 11 has been observed ([19]).

The most common attempts to solve the missing-satellite problem invoke baryonic physics and state that ([2]):

- The ultraviolet radiation could heat the halo gas and suppress gas accretion onto subhalos.
- Supernovae or stellar winds could drive most of the gas out of the subhalos.

Therefore, according to this model, Dark Matter small-sized halos do form, but baryonic matter is swept away or does not even settle over them, making it hardly impossible to directly probe the presence of Dark Matter subhalos. However, it is not clear if these solutions can explain the observations over the full range of halo and subhalo masses.

In FDM models, the missing-satellite problem is easy to solve thanks to equation (36). The number of low-mass FDM halos or subhalos is rapidly suppressed, so we do not expect to observe many. However, there is another reason that further reduces the expected number of FDM low-mass halos: the inevitable tidal disruption of subhalos, due to the upper limit on their density (described in equation (26)) and the possibility for FDM to tunnel through the potential barrier centered on the tidal radius. More precisely, a soliton cannot survive on a circular orbit on a host system for more than 10^{11} orbits, unless its central density is $\rho_c \gtrsim 60\rho_{host}$. However, the time required by a soliton to travel an orbit often exceeds the Hubble time. For example, the orbital period of the Sun is $\sim 2.25 \cdot 10^8$ y, so it takes $10^{11} \cdot \frac{2.25 \cdot 10^8}{14 \cdot 10^9} \sim 1.6 \cdot 10^9$ times the Hubble time to describe 10^{11} orbits. If the soliton mass were $\rho_c \gtrsim 100\rho_{host}$, then the survival time would decrease to a few hundred orbits. This limit has to be compared with the maximum density of FDM structures given by equation (26). Using these two relations, it is possible to estimate the minimum mass of an FDM structure that survives for 10 orbits with radius 10 kpc. We will suppose that the mass of the host galaxy is about $10^{11} M_\odot$: the same magnitude of the Milky Way mass.

$$M_{FDMstruct} > 6.7 \cdot 10^8 M_\odot \left(\frac{M_{host}}{10^{11} M_\odot}\right)^{\frac{1}{4}} \left(\frac{10\text{kpc}}{r_{host}}\right)^{\frac{3}{4}} \left(\frac{10^{-22}\,\text{eV}}{m}\right)^{\frac{3}{2}} \tag{40}$$

This limit remarks again the suppression of FDM structures with mass lower than $10^8 M_\odot$, and is consistent with simulations. The suppression on the number of FDM halos over the CMD ones becomes much more evident analyzing the power spectra of density fluctuations. In fact, as it will be shown in Section 4, the power spectrum of FDM density fluctuations is suppressed at small masses relative to CDM.

Currently, the most stringent observing limits come from the ALMA interferometer, which allows to analyze the gravitational lensing of high-redshift galaxies by dark matter subhalos and probe the subhalo mass function. The sensitivity of ALMA to subhalo masses is about $10^9 M_\odot$ [20], but this limit is expected to be reduced in the future.

The missing-satellite problem will be analyzed in greater detail in Section 6.

3.6 The too big to fail problem

Even assuming that the baryonic physics explanations for the mismatch between the observed number of dwarf galaxies and the predicted one are correct, a new problem arises. In fact, some of the expected galaxies are just so massive that there's no way they could not have visible stars. In other words, the dwarf galaxies orbiting around the Milky Way seem to have much less dark matter than the simulations would predict.

This conclusion was reached by Bullock et al. ([21]), who used standard abundance matching methods to relate galaxies and halos [4] to predict the magnitude difference between central and satellite galaxies in groups. A possible explanation involves feedback from massive stars and black hole outflows, but a definitive answer has not been reached yet.

Anyway, Fuzzy Dark Matter model smartly reduces the magnitude of the too big to fail problem through two phenomena. At first, as will be shown in Section 4, the number of halos with mass smaller than $10^{10} M_\odot$ is strongly suppressed in FDM model. Secondly, since the maximum circular speed of baryons is lower if they populate a FDM halo than a CDM one with the same mass, the measured value of the mass of a halo varies according to the adopted Dark Matter model. In other words, if FDM model is correct, the masses of the probed small-sized halos are lower than the measured ones, so that the halos may still not accommodate a visible dwarf galaxy.

[4] These methods permit to determine the subhalo masses through the measurement of the maximum circular speed of the baryons settled on them.

4 FDM suppression over small galaxy formation in the linear regime

All the graphs reported in this section are the result of simulations conducted with the code AXIONcamb([22], [23], [24]): a modified version of the more popular CAMB that computes cosmological observables for comparison with data. AXIONcamb exploits the Madelung Equations (23) to produce, among other results, simulated power spectra for Dark Matter - both CDM and FDM - density fluctuations. These power spectra P(k) have been studied varying the mass of FDM particles, the redshift, the mass of neutrinos, the ratio between the density of FDM and the global Dark Matter one and the density of Dark Matter Ω_D. It is of primary importance for the following to underline that ***all the results computed with AXIONcamb are obtained in the linear regime****.*

A remarkable difference between CDM and FDM regards the stability of density fluctuations. These are unstable over all spatial scales for CDM while, thanks to its large wavelength, FDM is stable for masses smaller than the Jeans mass. As shown in Section 3.3, because of the uncertainty principle, an increase in momentum opposes any attempt to confine FDM particles under the Jeans scale (with which the Jeans mass can be defined).

This fact brings to a strong constraint on the abundance of FDM low-mass halos. More precisely, the linear power spectrum of density fluctuations in FDM is strongly suppressed compared to CDM at small scales. A numerical result that reproduces this suppression was calculated by Hu, Gruzinov and Barkana ([1]):

$$\frac{P_{FDM}(k)}{P_{CDM}(k)} = T(k) \qquad \text{with} \qquad T(k) \approx \left(\frac{\cos(x^3)}{1+x^8}\right)^2 \tag{41}$$

where $x = 1.61 m_{22}^{1/18} \frac{k}{k_{Jeq}}$, with $k_{Jeq} = 9 m_{22}^{1/2} \mathrm{Mpc}^{-1}$ and $m_{22} = \frac{m_a}{10^{-22}\,\mathrm{eV}}$.
This ratio has also been probed in this thesis, resulting in the relation:

$$T(k) \approx \left|\frac{\cos(x^{2.7})}{1+x^{7.5}}\right|^{\frac{3}{2}} \tag{42}$$

The exponents 7.5 and 3/2 reproduce the slope of the suppression better, while the exponent of the argument of the cosine controls the position of the local minima. The choice of the exponent 2.7 is due to its better fitting with the simulation at nearly-half of the suppression (Figure 5). However, the T function fails in predicting the position of every local minima, so it needs to be further generalized. Moreover, as shown in Figure (5), even changing m_a the function (42) is still a good approximation of the slope of the simulation.

Furthermore, the proposed fit for $T(k)$ has been successfully tested for different Dark Matter densities Ω_D. As shown in Figure 6, simulations for $\Omega_D \cdot h^2 = 0.2, 0.4$[5] don't significantly differ from the fit.

[5]Corresponding to a Universe composed of 44.5% and 89% of Dark Matter respectively.

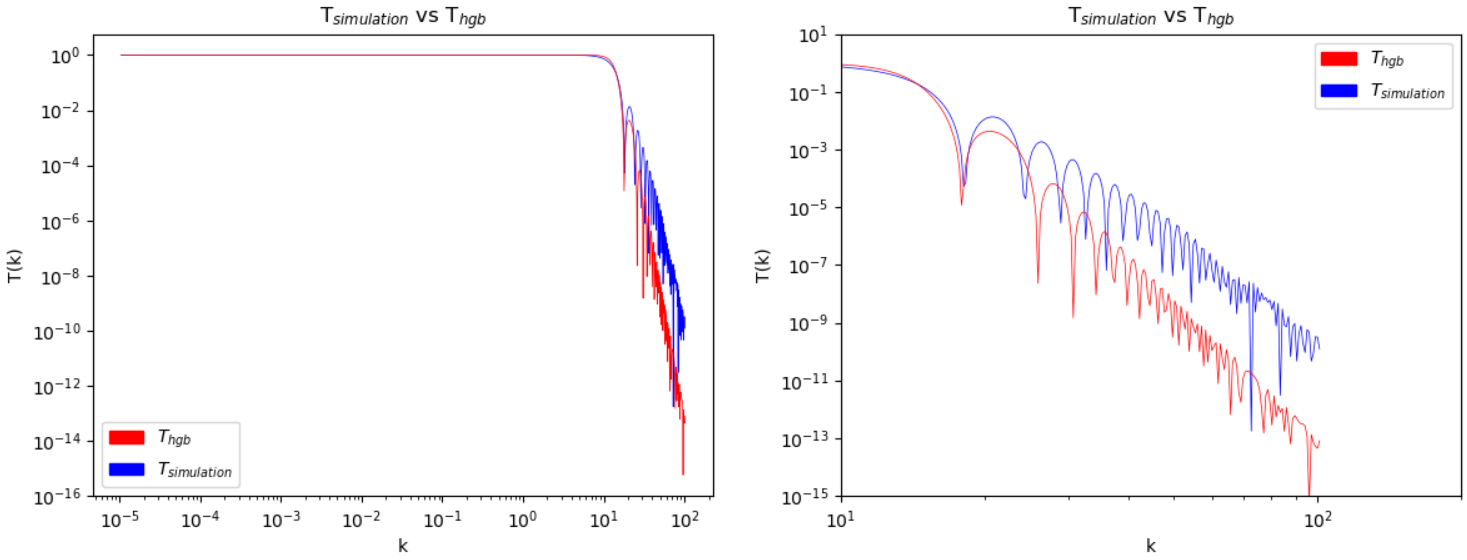

Figure 3: Comparison between the T function by Hu, Gruzinov and Barkana and the ratio of the power spectra of CDM and FDM given from a simulation for $m_a = 4 \cdot 10^{-22}$ eV

A further parameter whose influence on T function has been investigated is the neutrino mass, which has been made to vary within the range of $0.06\text{eV} < m_\nu < 0.6\text{eV}$. The results, that exclude any dependence of the T function on m_ν, are summarized in Figure 7.

According to equation (41), the FDM power spectrum is suppressed by a factor of 2 at

$$k_{1/2} \approx \frac{1}{2} k_{Jeq} m_{22}^{4/9} = 4.5 m_{22}^{4/9} \text{Mpc}^{-1} \tag{43}$$

which corresponds to the mass

$$M_{1/2} = \frac{4}{3}\pi\rho \left(\frac{\pi}{k_{1/2}}\right)^3 = 5 \cdot 10^{10} M_\odot \frac{\Omega_{FDM}}{0.27} m_{22}^{-4/3} \tag{44}$$

This suppression imposes a much more stringent limit on FDM halos than the one presented in Section 3.3 ($M \gtrsim 1.4 \cdot 10^7 M_\odot$).

Assuming that the rate of suppression has never changed[6], this result has a fundamental consequence: FDM tends to suppress the formation of small galaxies at high redshift compared to CDM. This fact offers an important opportunity to probe FDM models. In particular, it is necessary to verify if the FDM lower limit on Dark Matter halos is consistent with the high-redshift galaxy luminosity function, reionization at $z = 8 - 9$ and production of small-scale structures probed by the Lyman-α forest.

[6]This assumption will be tested later.

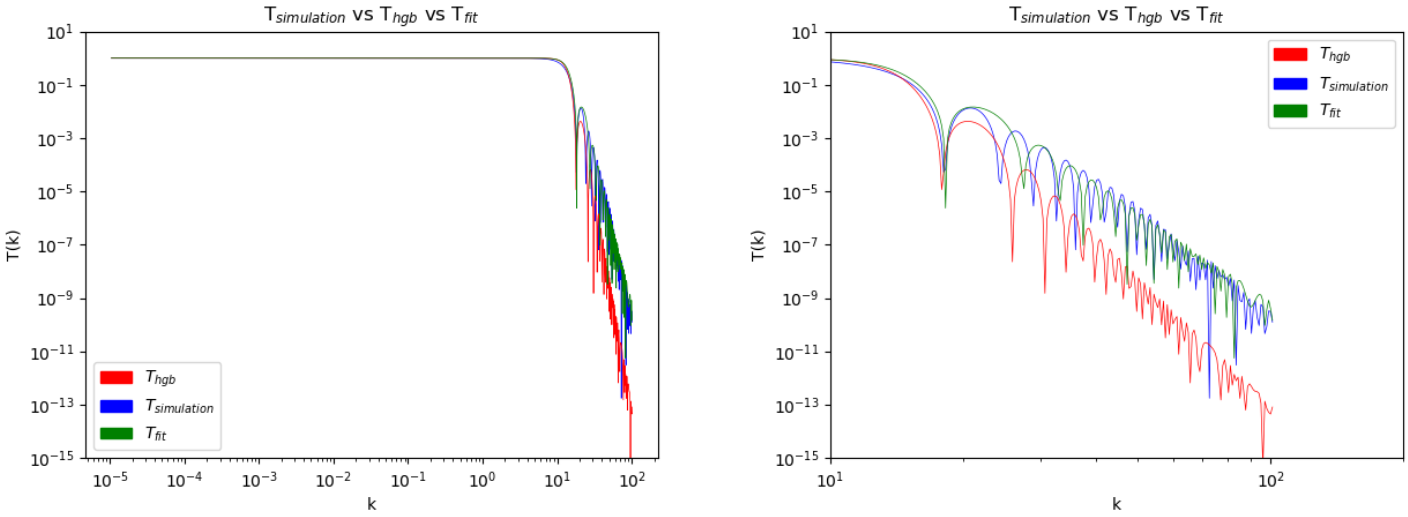

Figure 4: Comparison between the T function by Hu, Gruzinov and Barkana, the correction fit and the simulation for $m_a = 4 \cdot 10^{-22}$ eV

According to the limit (44) and noticing that $M_{1/2} \gg M_J \approx 1.4 \cdot 10^7 M_\odot$, it is possible to neglect any effect due to the wavy nature of FDM (that becomes important for $M \approx M_J$). Therefore, one can approximate the formation of structure in FDM using CDM simulations in which the initial power spectrum is that of FDM. However, these simulations ([25]) show that FDM is still able to reproduce the UV luminosity function of galaxies ad $z = 4 - 10$) and is consistent with current observations of the reionization history. Consistence between FDM lower limit on halos and the production of small-scale structures are discussed in the next section.

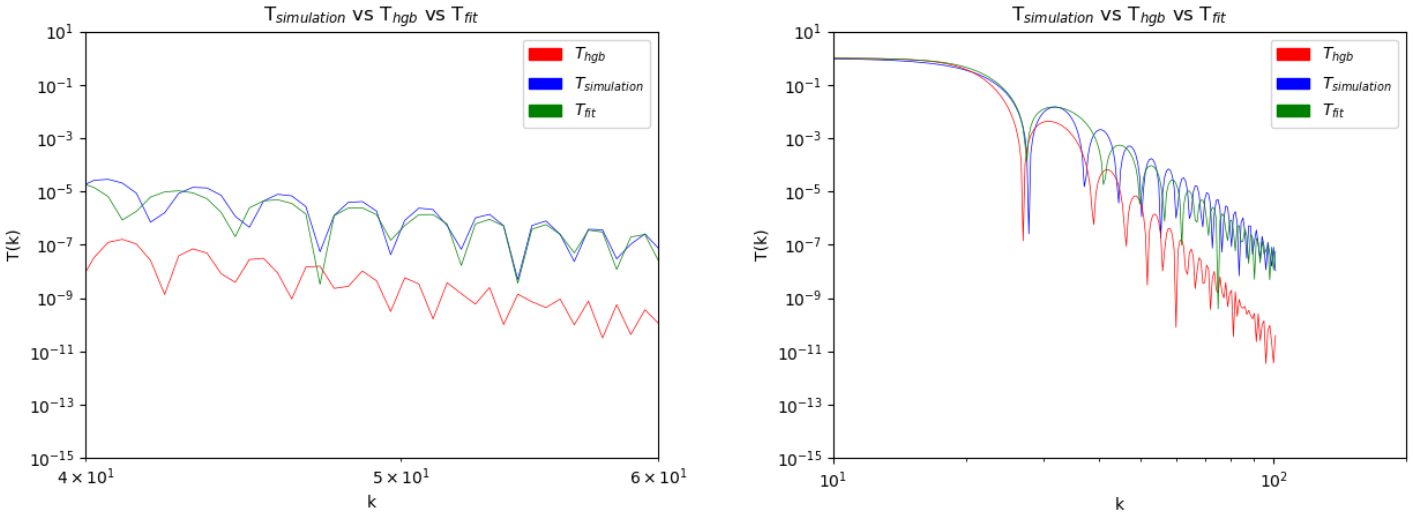

(a) (b)

Figure 5: Comparison between the T function by Hu, Gruzinov and Barkana, the correction fit and the simulation for $m_a = 4 \cdot 10^{-22}$ eV (a) and $m_a = 10 \cdot 10^{-22}$ eV (b)

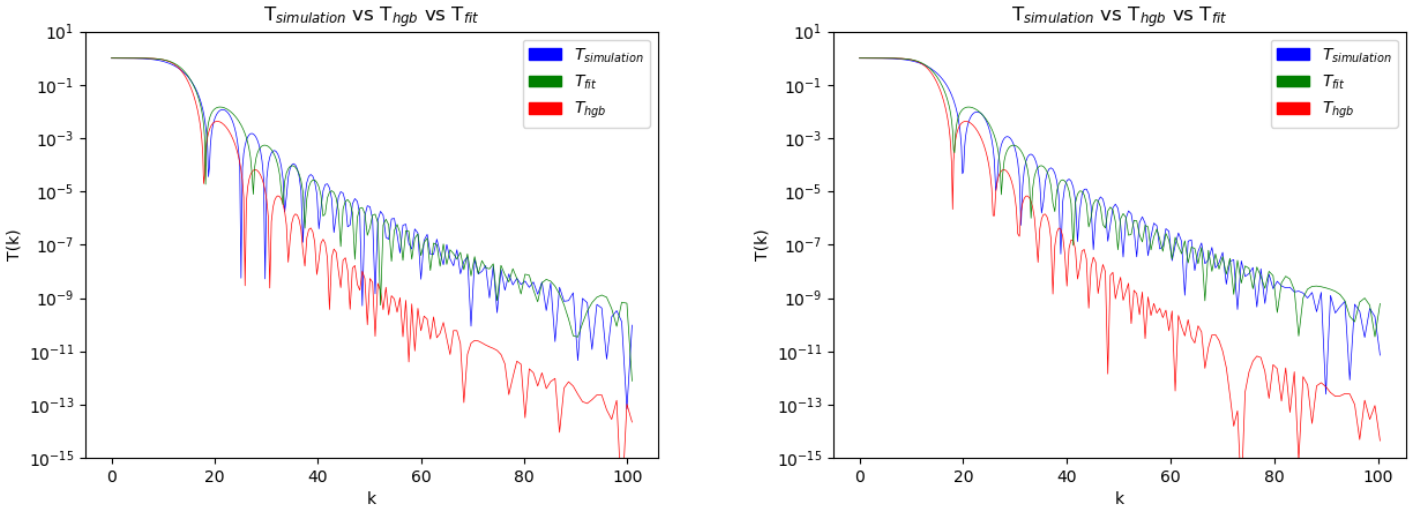

(a) (b)

Figure 6: Comparison between the T function by Hu, Gruzinov and Barkana, the correction fit and the simulation for $m_a = 4 \cdot 10^{-22}$ eV for $\Omega_D \cdot h^2 = 0.2$ (a) and $\Omega_D \cdot h^2 = 0.4$ (b)

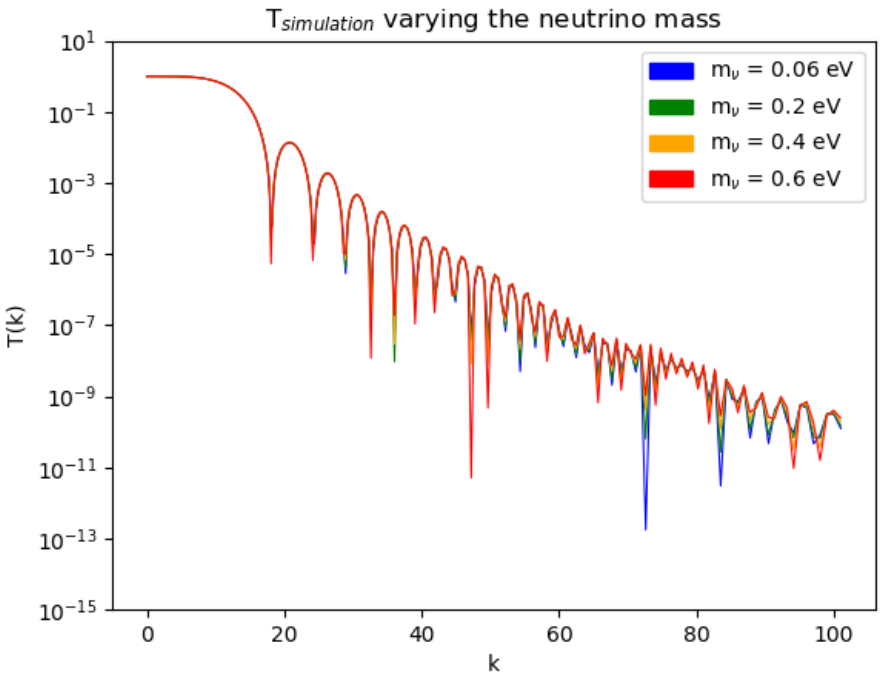

Figure 7: Overlap of the T functions for several values of m_ν.

5 Constraints on FDM due to the Lyman-alpha forest

Currently, the most stringent constraint on FDM, that threats to rule out the entire model, comes from the Lyman-alpha forest. In the following, a first explanation about what the forest is and how can it bind the FDM model is given. Hence, a detailed comparison between the data provided by the Lyman-alpha forest and both the FDM and the alternative "mixed" solution is presented.

5.1 The Lyman-alpha forest

The nature of the Lyman-alpha forest can be understood starting from the light emitted from quasars. In particular, quasars emit energy in the whole electromagnetic spectrum, including a strong Lyman-alpha emission line at $\lambda = 122\,\text{nm}$. However, the typically huge redshift of quasars makes sure that the observed Lyman-alpha line is shifted to a major wavelength.

The Lyman-alpha forest forms when the light emitted from a far quasar crosses at least one of the numerous clouds of gas that stands between the quasar and the Earth. The intergalactic clouds absorb the ultraviolet light of the Lyman-alpha transition but, being at a smaller distance from Earth, the redshift of the absorption line is smaller. Therefore, all the spectrum absorption lines due to the intergalactic clouds are in the shorter wavelength side of the quasar emission line. Since there are many absorbing clouds, the resulting spectrum is composed of the initial emission line, followed by some identical absorption lines at different redshift. The process is summarised in the following picture

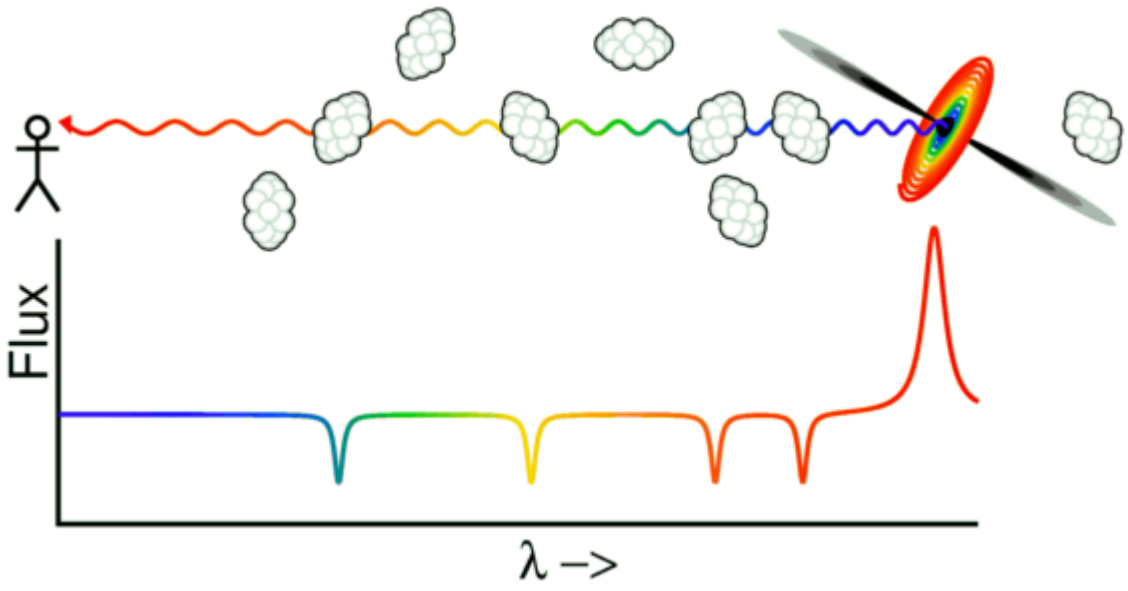

while below are two examples of spectra of high redshift objects

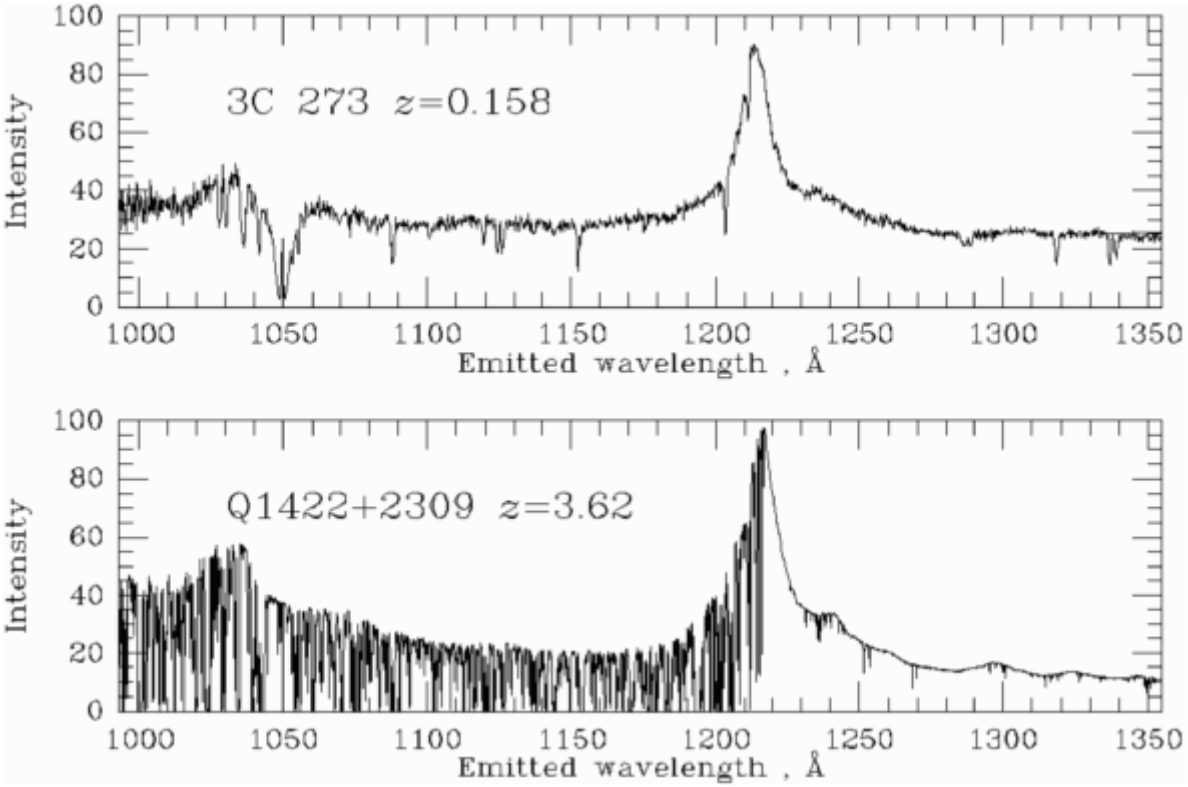

5.2 Contraints on FDM

The Lyman-alpha forest represents an extremely useful method for probing the matter power spectrum at small scales ($0.5\text{Mpc/h} \lesssim \lambda \lesssim 100\text{Mpc/h}$), at which the intergalactic medium displays structures ([26]). This is possible thanks to the fact that the Lyman-alpha forest is composed of many contributors from clouds at different redshifts. Therefore, it is possible to analyze the evolution of these structures, which is affected by the characteristics of Dark Matter. This approach is also useful to probe FDM models. In fact, even though the de Broglie wavelength is rather small, the effect of FDM on the linear power spectrum is noticeable on scales larger than the smallest scales typically constrained by intergalactic medium data. Moreover, the quantum pressure term in equation (23) results to have a negligible effect on the structure formation relevant for the Lyman-alpha forest.

However, although there are no reasons to suppose that the rate of suppression of CDM density fluctuations on FDM ones has ever changed, it is necessary to probe this hypothesis using simulations. In Figure 8, some $T(k)$ functions are presented for different redshifts:

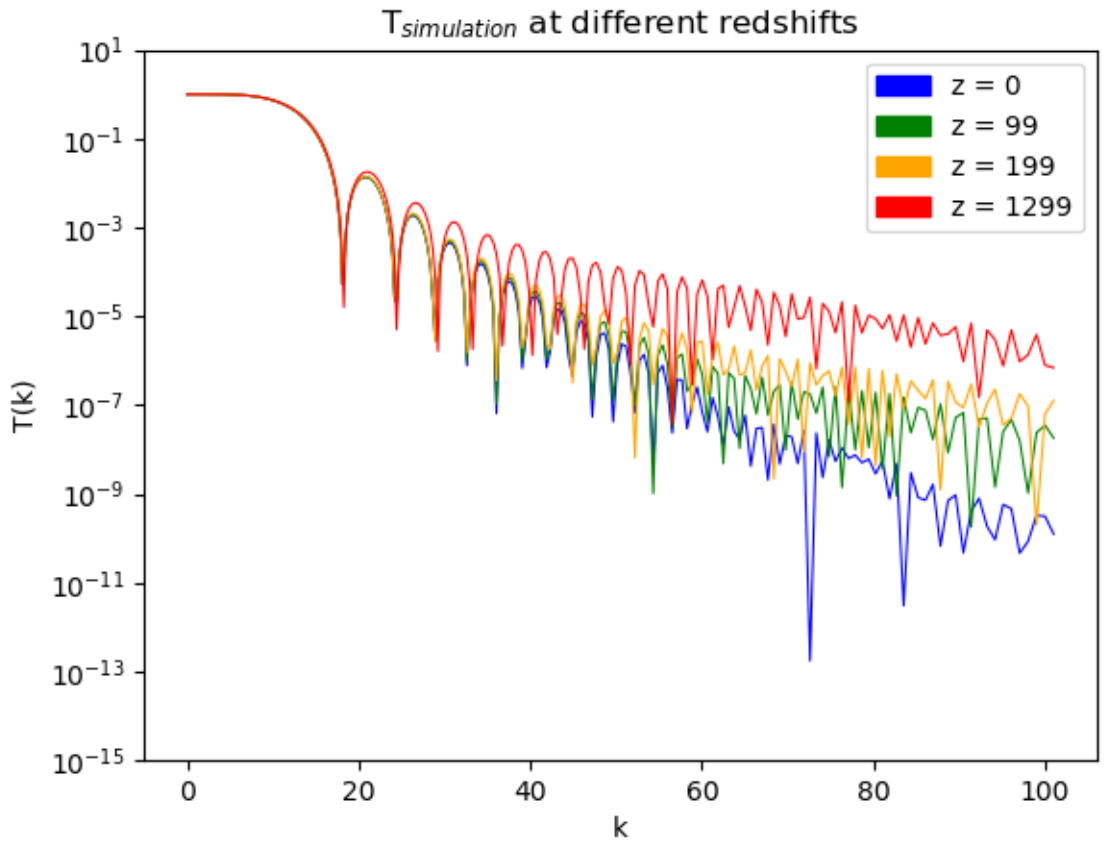

Figure 8: T function at different redshifts.

Therefore, although some dependence of T from the redshift emerges, it can be neglected when probing the Lyman-alpha forest constraints since the furthest objects that contributes to the forest have $z \approx 10$.

The method for probing Dark Matter through the Lyman-alpha forest is broadly the following:

1. At first it is necessary to follow the evolution of structures in the selected model using collisionless N-body simulations.

2. An artificial Lyman-alpha forest spectrum is extracted from the data produced with the simulation.

3. The artificial spectrum is compared with the observed one, and the match (or mismatch) permits to corroborate (reject) the model.

4. The process is iterated varying some parameters of the initial model in order to find the constraints.

Following this approach, Irŝiĉ et al. ([27]) used hydrodynamical simulations to model the Lyman-alpha power spectrum in the FDM model and compared it with the observed flux of the quasars XQ-100 and HIRES/MIKE. This analysis brought to a very strong constraint over the mass of FDM particles:

$$m_a > 20 \cdot 10^{-22}\,\text{eV} \tag{45}$$

which seems to make vain every attempt to solve the Cold Dark Matter small scale crisis with ultralight particles, inasmuch it clashes with the expected values for m_a calculated in Section 3.1. This result will be further analyzed in Section 6.

However, an alternative solution was recently proposed by Kobayashi at al. ([28]). In particular, even though FDM alone can't explain the data provided by the Lyman-alpha forest, a mixed model, in which both Fuzzy and Cold Dark Matter constitute the entire Dark Matter, could still be valid. In fact, defining the ratio $F = \frac{\rho_{FDM}}{\rho_{TOT}}$ between the densities of FDM and total Dark Matter, it is possible to obtain new and less restrictive constraints. The results are represented in Figure 9

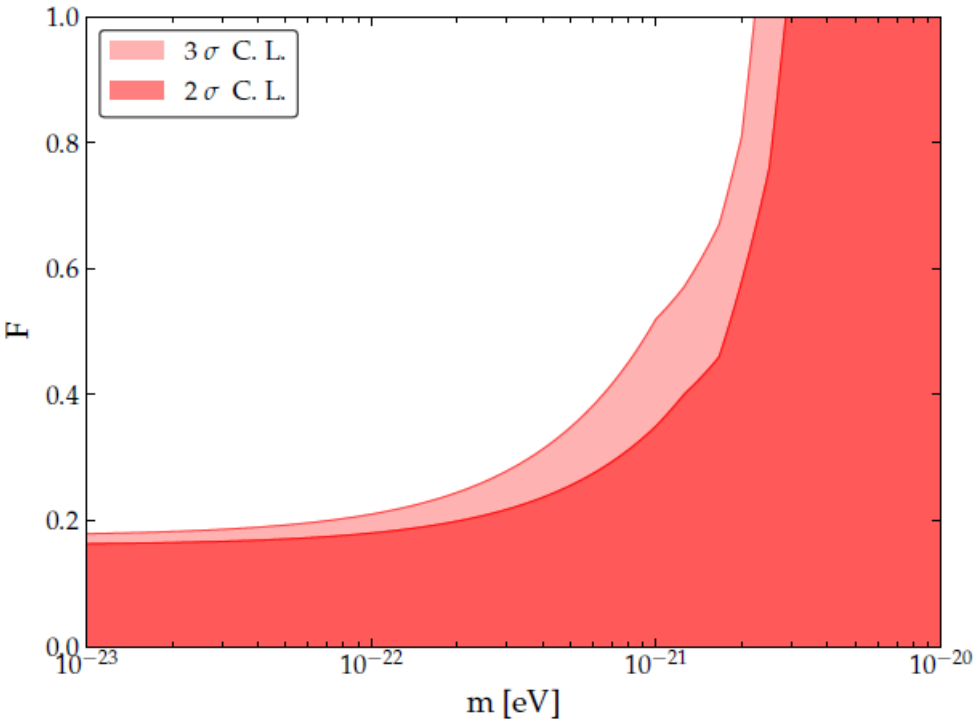

Figure 9: Constraints on the mass of FDM particles for mixed models with density ratio F ([28]).

Therefore, although for $F > 0.4$ FDM is ruled out (since the constraint $m_a \gtrsim 10^{-21}\,\text{eV}$ clashes with the values estimated in Section 3.1), it is recovered for lower F and can still be used to face the small scale crisis. Moreover, the Lyman-alpha forest

data are compatible with every value of m_a for $F \lesssim 0.2$.

Furthermore, the suppression of FDM power spectrum over Light Cold Dark Matter (LCDM) was studied again, now assuming that the Dark Matter isn't consisting of FDM entirely but is composed of both FDM and LCDM in a certain ratio F. Results are summarised in Figure 10. As expected, the suppression for $F = 1$ reproduces the original trend.

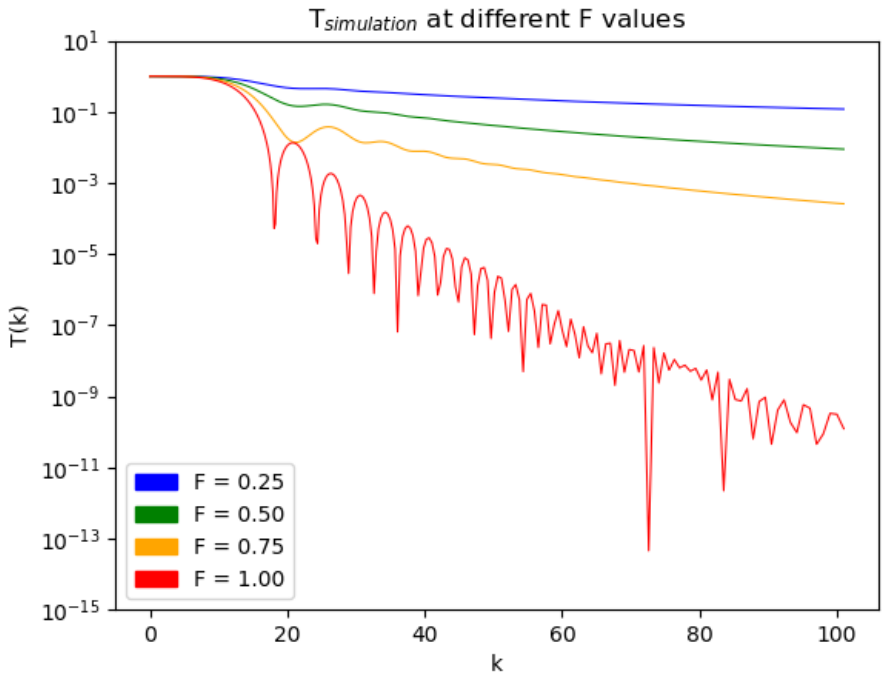

Figure 10: Suppression of FDM power spectrum over LCDM for different F values.

5.3 Full analysis of the missing-satellite problem

5.3.1 The extended Press-Schecther model

Although models with low F satisfy the Lyman-alpha forest constraints, it is necessary to verify if they can also solve the problems reported in Section 3. In this section, a formula estimating the expected number of CDM subhalos will be derived and used to show that the FDM model is unable to solve the missing-satellite problem while remaining compatible with the Lyman-alpha forest even for $F < 1$.

Many aspects of nonlinear structure formation, such as the FDM subhalos, can be analytically described by the extended Press-Schechter (EPS) model, which assumes *linear growth of perturbations followed by immediate halo formation above a certain threshold.* In particular, the threshold for the halo formation could be derived from an idealised

spherical collapse calculation. Obviously, these are oversimplified hypotheses, but nevertheless the model reproduces fundamental statistics of the structure formation. The main constraint on the EPS model comes from the initial power spectrum of CDM density fluctuations, which must not be steeper than k^{-3} to reproduce the right clustering. The formalism needs to be adapted in order to give adequate predictions for models with general initial power spectra. A first attempt of generalization was presented by Schneider et al. in 2013 ([29]), and the same method will be followed here.

The starting point of the EPS model is the halo mass function (originally presented in 1974 by Press and Schechter [30]):

$$\frac{dn}{d\ln M} = \frac{1}{2}\frac{\rho}{M} f(\nu) \frac{d\ln \nu}{d\ln M} \tag{46}$$

where n is the number density of haloes, M the halo mass, ν the peak-height of perturbations, ρ the average density of the universe and $f(\nu)$ is the first crossing distribution depending on the way one follows to model the collapse. For the spherical collapse $f(\nu)$ takes a particular simple shape ([31]):

$$f(\nu) = \sqrt{\frac{2\nu}{\pi}} e^{-\frac{\nu}{2}} \tag{47}$$

Finally, it is possible to bound ν to the other physical quantities through the equation:

$$\nu = \frac{\delta_{c,0}^2}{S(R)D^2(a)} \tag{48}$$

where $\delta_{c,0} = 1.686$, $D(a)$ is the universal growth factor of perturbations

$$D(a) = \frac{5\Omega_m}{2} H(a) \int \frac{da}{a^3 H(a)^3} \qquad \text{where} \qquad H = \frac{\dot{a}}{a} \qquad \text{is the Hubble parameter} \tag{49}$$

and finally $S(R)$ is the variance of a halo with radius R, defined as:

$$S(R) = \int \frac{d^3k}{(2\pi)^3} P(k) W^2(k|R) \tag{50}$$

where $P(k)$ is the *linear* power spectrum ([32]) and $W(k|R)$ is a filter function in Fourier space that takes into account the threshold mentioned before. There are many possible choices for W: a first possibility is a top-hat function in real space with enclosed mass $M = \frac{4\pi\rho R^3}{3}$, i.e.

$$W(k|R) = \frac{3}{(kR)^3}[\sin(kR) - 3\cos(kR)] \tag{51}$$

in Fourier space. The resulting EPS halo mass function is in very good agreement with CDM simulations for halo masses below $M = 10^{13} M_\odot/h$, and needs to be slightly modified for bigger masses ([33]).
However, different W filters lead to only slightly different models. In particular, since

the top-hat filter used in the standard EPS approach is unable to model cosmologies with strongly suppressed power spectra, it could be convenient to confer another shape to W:

$$W(k|R) = \Theta(1 - kR) \tag{52}$$

where Θ is the Heaviside step function. This elegant simplification, introduced by Bertschinger in 2006 ([34]), consists in switching the filter from a top-hat function in the real space to a top-hat function in the Fourier space. Formula (52) goes by the name of *sharp-k filter*. Adopting this filter, the halo mass function can be simplified:

$$\frac{dn}{d\ln M} = \frac{1}{12\pi^2}\frac{\rho}{M}\nu f(\nu)\frac{P(1/R)}{\delta_c^2 R^3} \tag{53}$$

Moreover, the sharp-k filter has no well defined mass M associated to its filter scale R. Therefore, the halo mass is unconstrained, and its dependence on R could be reproduced as:

$$M = \frac{4\pi}{3}\rho(cR)^3 \tag{54}$$

In other words, we expect that $M \propto R^3$ due to the spherical symmetry, but we also reserve the right to adjust the constant of proportionality c in order to make equation (54) match with observational data. This approach suggests that $c = 2.5$ is the best choice.

The most important application of the EPS model for the purposes of this thesis is the conditional mass function: a formula that gives the abundance of haloes per mass. In particular, the conditional mass function is given by ([35]):

$$\frac{dN(M|M_0)}{d\ln M} = -\frac{M_0}{M}Sf(\delta_c, S|\delta_{c,0}, S_0)\frac{d\ln S}{d\ln M} \tag{55}$$

and it can be simplified adopting a sharp-k filter:

$$\frac{dN(M|M_0)}{d\ln M} = \frac{1}{6\pi^2}\frac{M_0}{M}f(\delta_c, S|\delta_{c,0}, S_0)\frac{P(1/R)}{R^3} \tag{56}$$

where, as before, the first crossing distribution f depends on the assumed model for nonlinear collapse. For a spherical collapse,

$$f(\delta_c, S|\delta_{c,0}, S_0) = \frac{(\delta_c - \delta_{c,0})}{\sqrt{2\pi(S - S_0)}}\exp\left[-\frac{(\delta_c - \delta_{c,0})^2}{2(S - S_0)}\right] \tag{57}$$

obtained by shifting the starting point of trajectories from $(0, 0)$ to $(\delta_{c,0}, S_0)$ in the $(\delta_c - S)$ plane.

This approach can be used to estimate the average dwarf galaxies orbiting a galaxy (the Milky Way, in the following). However, one must remember that this estimate comes from an over-simplification: finding the number of a halo progenitors should require the construction of the full merger-tree, i.e. for every halo one should consider all the possible

mergers of pre-existing haloes that could have formed the considered halo. However, because of the complexity of this calculus, one could follow a simplified procedure (firstly adopted by Giocoli et al. [36]) and estimate the total number of progenitors over all redshifts $N_{sat}(\delta_c > \delta_{c,0})$ by computing the following integral:

$$\frac{dN_{sat}}{d\ln M} = \frac{1}{N_{norm}} \int_{\delta_{c,0}}^{\inf} \frac{dN}{d\ln M} d\delta_c \tag{58}$$

The reason why one must introduce the normalization constant N_{norm} is because the integral overestimates the actual number of progenitors (and thus the expected number of substructures) because it includes multiple counts pf structures simultaneously existing at different redshifts. This issue can be solve just by fixing N_{norm} so that (58) is in agreement with the outcome of the ΛCDM simulations. This leads to $N_{norm} = 44.5$. Therefore, for a sharp-k filter, the expected number of satellites is given by:

$$\frac{dN_{sat}}{d\ln M} = \frac{1}{44.5} \frac{1}{6\pi^2} \frac{M_0}{M} \frac{P(1/R)}{R^3\sqrt{2\pi(S-S_0)}} \tag{59}$$

resulting in

$$\frac{dN_{sub}}{dM_{sub}} = \frac{1}{44.5(6\pi)} \frac{M_{halo}}{M_{sub}^2} \frac{P(1/R_{sub})}{R_{sub}^3\sqrt{2\pi(S_{sub}-Shalo)}} \tag{60}$$

where R, M and S are the radius, mass and variance of the main halo or of a given subhalo defined as:

$$S_s = \frac{1}{2\pi} \int_0^{1/R_i} dk k^2 P(k), \qquad M_i = \frac{4\pi}{3} \Omega_m \rho_c (c \cdot R_i)^3, \qquad c = 2.5 \tag{61}$$

where $P(k)$ is the linear power spectrum of a given model at $z = 0$ and ρ_c is the critical density today.

However, before proceeding with the calculus in the following, it is important to remark the limits of formula (60). First of all, it is obtained for the linear regime only, and should be adjusted for the nonlinear regime for a more accurate analysis. Secondly, the entire model is clearly an over-simplification and does not take into account the full hierarchical structure formation process. Moreover, due to the simplified method followed to obtain equation (58), the model does not give the final subhalo mass prior to the merger with the host, but rather some average mass of the subhalo formation history. Finally, it does not consider the tidal striping, which could significantly reduce the mass of a substructure whenever it approaches the main halo.

5.3.2 Explicit calculus of the expected number of FDM subhaloes

According to the constraints imposed by the Lyman-alpha forest and the missing-satellite problem, the value $m_{22} = 25$ should be one of the very few that satisfy both the issues. However, before proceeding with the calculus, it is important to remind that equations (60) and (61), that allow us to estimate the expected number of satellites for a given

value of m_{22}, are derived in linear approximation. On the other hand, the constraint given from the Lyman-alpha forest is derived in nonlinear approximation. However, although the most accurate estimate of the number of satellites should be derived in nonlinear approximation, a model that computes the number of satellites in nonlinear approximation has not been developed yet. Therefore, the FDM power spectrum P(k) that is going to be used is derived in *linear approximation* for $m_{22} = 25$: a value that has been proved to be hardly compatible with the Lyman-alpha forest in *nonlinear approximation*.

Firstly, the linearization of P(k) is obtained through the software Wolfram Mathematica ([17]). The results are shown in Figure 11.

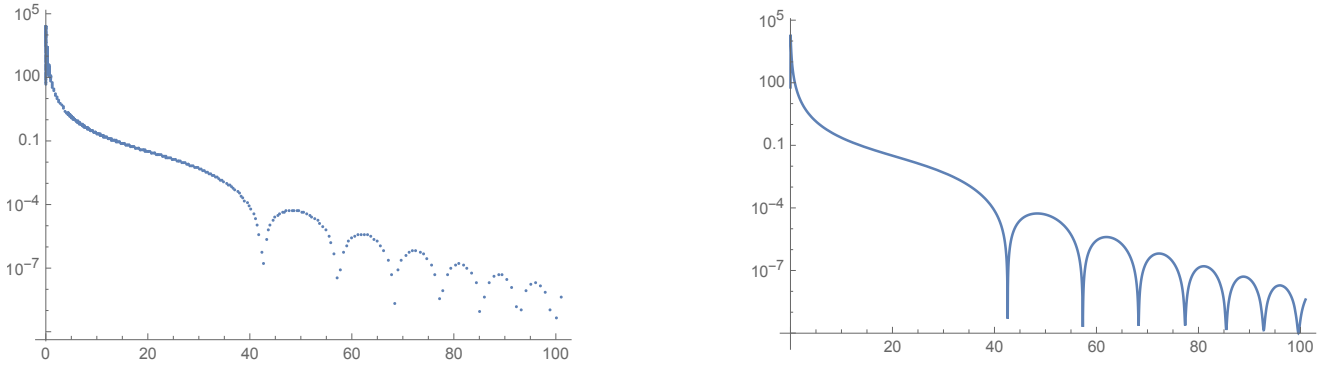

(a) (b)

Figure 11: Plot (a) and linearization (b) of the FDM power spectrum P(k) for $m_{22} = 25$. (Plot computed with Wolfram Mathematica ([17])).

Then, the dependence of the radius and variance of a halo on its mass was explicited through formulas (61).

$$R(M_i) = \frac{1}{c}\left(\frac{3M_i}{4\pi\omega_m\rho_c}\right)^{\frac{1}{3}}, \qquad S_i = \int_0^{\frac{1}{R(M_i)}} dk k^2 P(k) \tag{62}$$

Where P(k) was approximated with its linearization. This has made it possible to calculate the variance $S_{halo} = 72.37$ associated to a Milky Way-like halo with mass $M_{halo} = 1.7 \cdot 10^{12} M_\odot/h$. Finally, equation (60) was used to calculate the expected number of FDM subhalos with $10^8 M_\odot/h < M_{sub} < 10^{10} M_\odot/h$.

$$N_{sub} = \int_{10^8 M_\odot/h}^{10^{10} M_\odot/h} \left[\frac{1}{44.5 \cdot 6 \cdot \pi^2}\frac{M_{halo}}{M_{sub}^2}\frac{P(1/R(M_{sub})}{R(M_{sub})^3\sqrt{2\pi(S(M_{sub}) - S(M_{halo})}}\right] dM_{sub} \tag{63}$$

The described procedure led to the conclusion that $N_{sub} = 85.7$: a better result than the one obtained with standard CDM models, but still far from the observed 11 dwarf galaxies orbiting around the Milky Way. This result could be tainted by the roughness

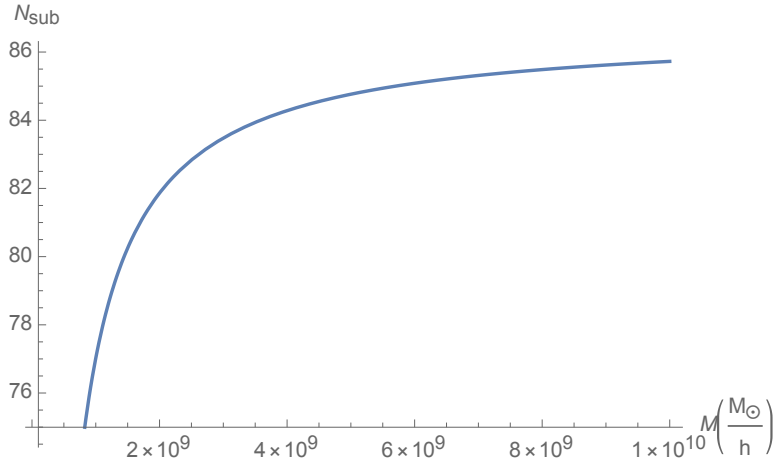

Figure 12: Expected number of subhalos with $10^8 M_\odot/h < M_{sub} < M$ for $M_0 = 1.7 \cdot 10^1 2 M_\odot/h$ and $m_{FDM} = 2.5 \cdot 10^{-21}$ eV. (Plot obtained using Wolfram Mathematica ([17]))

of the linearization reported in Figure 11 or from the over-simplified EPS model, but is in agreement with the conclusion reached by Kobayashi et al. ([28]): a FDM model with $m_{22} > 20$, i.e. compatible with the Lyman-alpha forest, is unable to solve the missing-satellite problem.

To get an idea of how the number of expected satellites varies according to their mass, one could define the following function:

$$N_{sub}(M_{max}) = \int_{10^8 M_\odot/h}^{M_{max}(M_\odot/h)} \left[\frac{1}{44.5 \cdot 6 \cdot \pi^2} \frac{M_{halo}}{M_{sub}^2} \frac{P(1/R(M_{sub})}{R(M_{sub})^3 \sqrt{2\pi(S(M_{sub}) - S(M_{halo})}} \right] dM_{sub} \tag{64}$$

which computes the expected number of satellites with mass in the range $10^8 M_\odot/h < M < M_{max}$. One could therefore plot (64), as in Figure 12, and check that it follows the expected behavior: the more a subhalo is massive, the less probable is its formation.

In ([28]), the missing-satellite problem is also faced with a mixed model: taking the Milky Way halo mass $M_{halo} \approx 1.7 \cdot 10^{12} M_\odot/h$ and considering subhalos with $M_{sub} \geq 10^8 M_\odot/h$ it is possible to obtain the predicted number of subhalos in function of m_a and F. The resulting N_{sub} is compared with the number of subhalos predicted by thermal Warm Dark Matter models with $2\,/\text{kilo/eV} < m < 3\,\text{keV}$ according to the same method, which has already been discussed in the literature as a solution to the missing-satellite problem. In particular, it is expected that $20 < N_{sub} < 30$. The result is summarized in Figure 13.

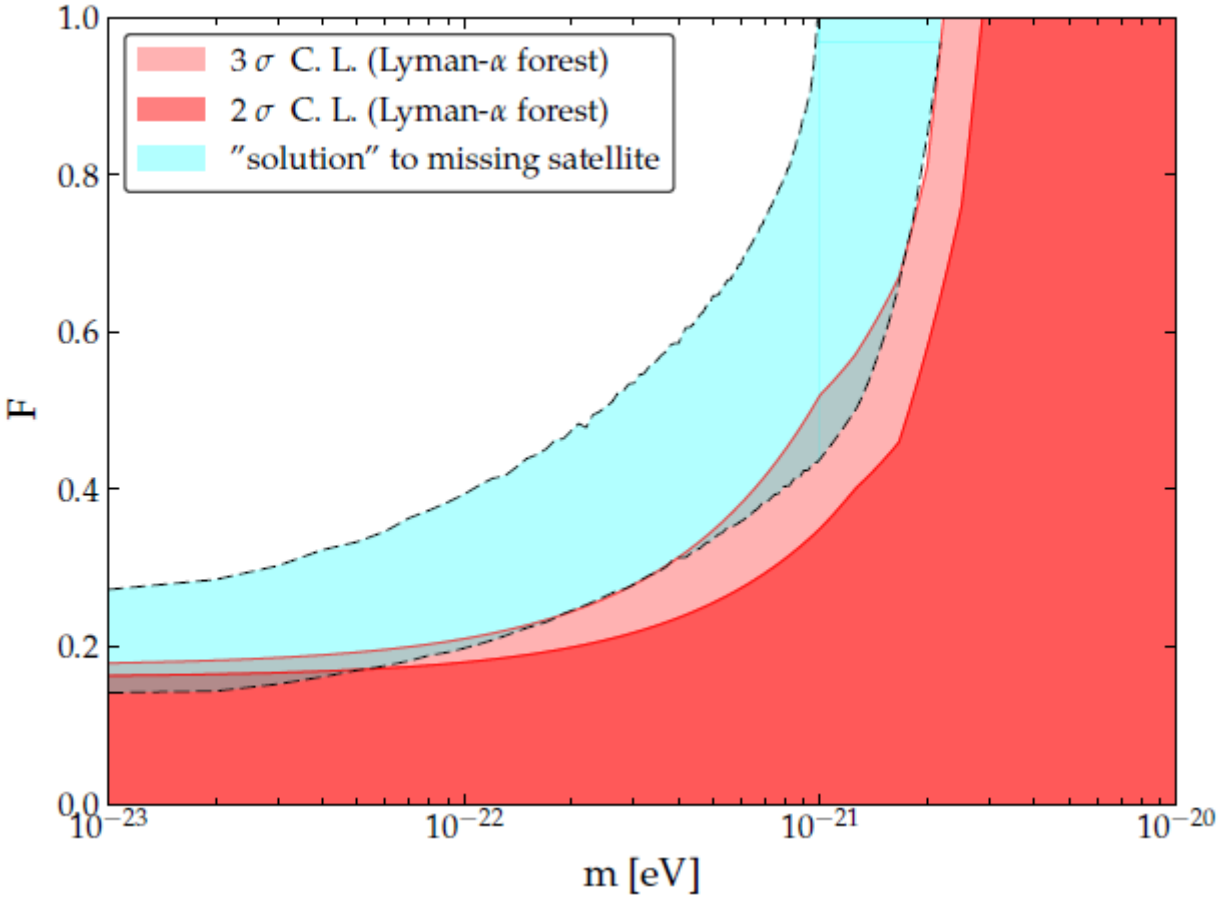

Figure 13: Comparison between the constraints on FDM mixed models imposed by the Lyman-alpha forest and the missing-satellite problem ([28]).

Therefore, the only remaining (m,F) values that are still in agreement with the Lyman-alpha forest with a confidence level lower than 2σ and together are able to solve the missing-satellite problem are confined in two very small areas: one with $m_a \approx 10^{-21}$ eV, already previously excluded, and one with $m_a \approx 10^{-23}$ eV and a very thin range of F values.

6 FDM suppression in the nonlinear regime

Unlike the graphs presented in the previous two sections, the following charts are obtained using AX-GADGET ([37], [38]): a new module of the parallel N-Body code P-GADGET3 for cosmological simulations of Fuzzy Dark Matter.

Every result reported in Section 4 and 5 was obtained through simulations conducted in the linear regime. However, the results seem to rule out the FDM model, as it fails to reproduce a Lyman-alpha forest compatible with the observed ones. Likewise, mixed models that are able to reproduce the forest cannot concurrently solve the missing-satellite problem. This section aims to summarise and evaluate the results obtained through simulations in the nonlinear regime.

In Section 5.2, a strong constraint on the mass of FDM particles was reported: $m > 2 \cdot 10^{-21}$ eV. This result was obtained by Irŝiĉ et al. ([27]) by comparing the artificial Lyman-α flux power spectrum obtained through hydrodynamical simulations with the observed flux power spectrum of two different observed Lyman-α forests. In particular, this constraint was obtained through simulations in the nonlinear regime.

In this Section, the suppression of FDM over Light Cold Dark Matter is analyzed in the nonlinear regime. More precisely, the suppression for $m_{22} = 2.5, 5, 25$ is evaluated at redshift $z = 2, 3.8, 5.4$. A first result is reported in Figure 14:

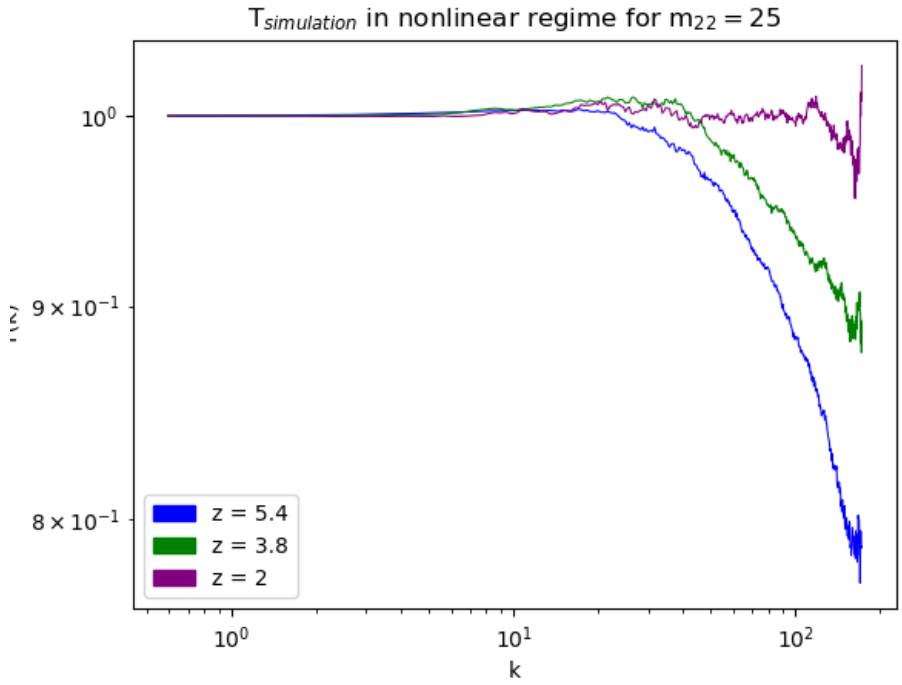

Figure 14: Suppression of FDM power spectrum over LCDM in the nonlinear regime for $m_{22} = 25$ at different redshifts.

Firstly, it is possible to notice that there is less suppression than in the linear regime, which is a remarkable fact, inasmuch the Lyman-α forest is not compatible with FDM in the linear regime because of its impossibility to form small scale structures. This is in agreement with what was expected: the non-linearity couples different scales and cancels primordial informations, therefore the linear suppression should be reproduced only for redshifts much higher than 5.4. Another interesting feature concerns the relation between the redshift and the suppression: as shown in Figure 8, in the linear regime a higher redshift is associated with a lower suppression, although the dependence is very weak, while in the nonlinear regime the higher is the redshift the higher is the suppression. Moreover, as expected, the dependence of the suppression by the redshift is much more marked in the nonlinear regime. The same considerations are valid for other masses, presented in Figure 15.

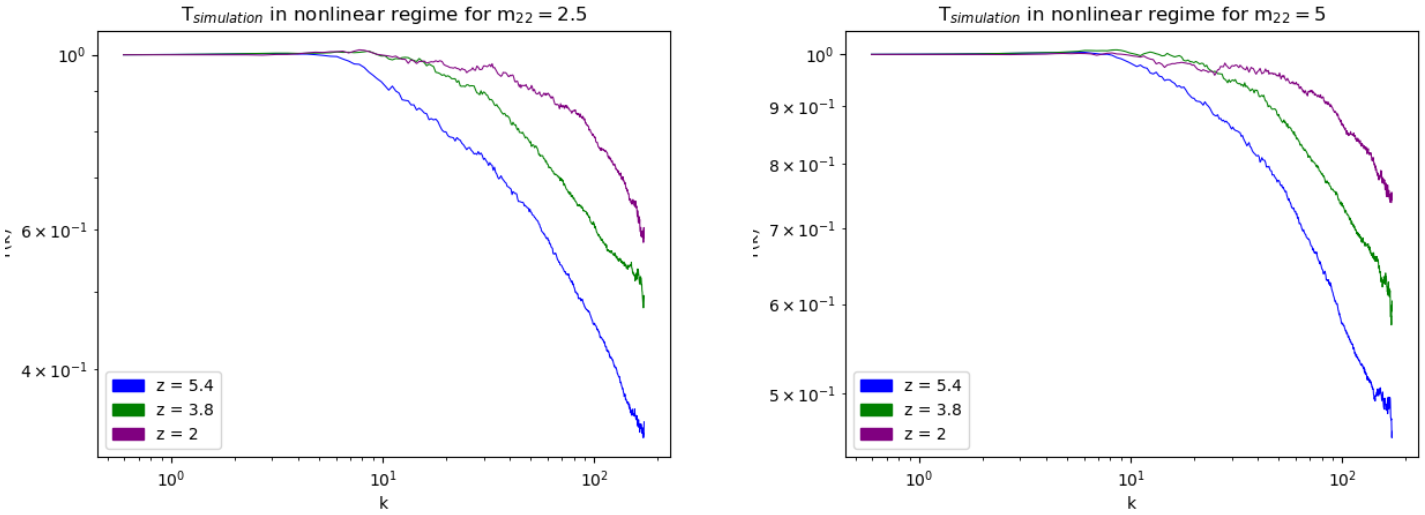

(a) (b)

Figure 15: Suppression of FDM power spectrum over LCDM in the nonlinear regime for $m_{22} = 2.5$ (a) and m_{22} at different redshifts (b).

It is also possible to observe the dependence of the suppression on the mass at fixed redshift from Figure 16.

Again, the nonlinear simulation is in agreement with the expected behaviour of FDM: a higher value of the mass is associated with a smaller De Broglie wavelength, and consequently the scale over which the formation of FDM structures is inhibited becames also smaller. However, as previously reported, the values $m < 10^{-22}$ eV are ruled out by the Lyman-α forest, therefore - among the analyzed ones - only $m = 25 \cdot 10^{-22}$ eV can be a good value for the mass of FDM particles, but it has been shown in 5.3.2 that this value can't solve the missing-satellite problem.

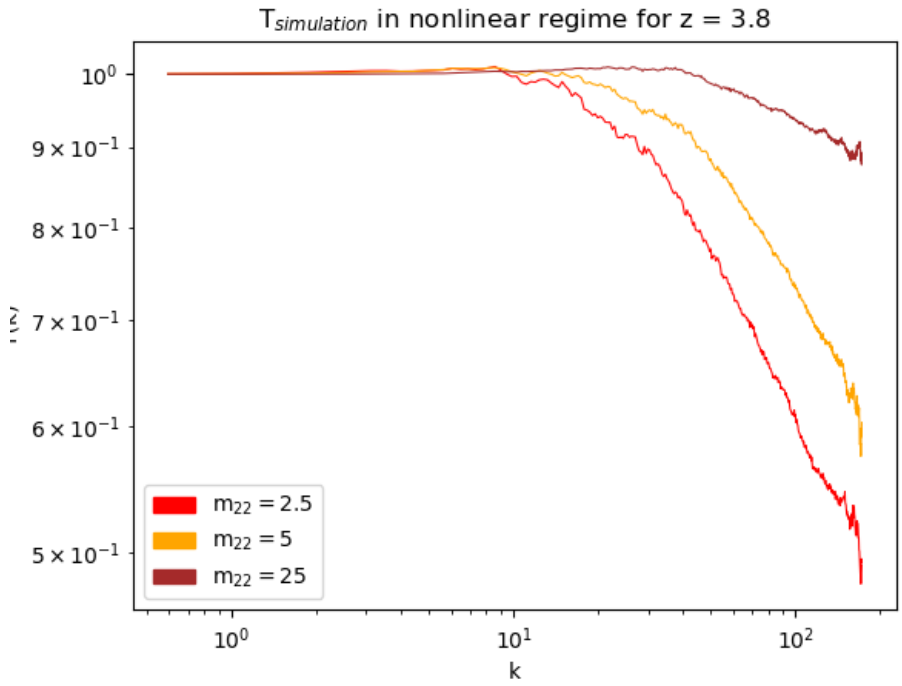

Figure 16: Suppression of FDM power spectrum over LCDM in the nonlinear regime at $z = 3.8$ for different masses.

7 Summary and Conclusions

In this work, the Fuzzy Dark Matter model was presented and analyzed as a possible solution of the small-scale crisis of Dark Matter. After an overall introduction, the physics that describes the properties of FDM particles was summarized. In particular, a reasonable value for m_{FDM} was shown to be $\sim 10^{-21} - 10^{-22}$ eV. Hence, a lower limit on the size of an FDM structure was derived for a Milky Way-like halo: $r_{FDM} \gtrsim 0.335$ kpc. Similarly, an upper limit to FDM structures central density and a lower bound on their masses are calculated: $\rho_{FDM} \lesssim 7.05 M_\odot \mathrm{pc}^{-3}$ and $M_{FDM} \gtrsim 1.5 \cdot 10^7 M_\odot$. Moreover, effects due to the relaxation of bond structures in systems composed of FDM were analyzed, but the time that these phenomena require to produce observable effects is usually much longer than the typical age of the same structures. Thus, the three issues that constitute the small-scale crisis (cusp-core problem, missing-satellite problem and too big to fail problem) were presented and analyzed.
The FDM suppression over small-scale structure formation is the main feature that distinguishes FDM from CDM, and the one that could hopefully solve the small-scale crisis. Therefore, the ratio of FDM and CDM power spectra was derived using numerical simulations in the linear regime and reported in Section 4. A first original result presented in this thesis consists of an improved formula describing the suppression of the two power spectra (based on the one originally derived by Hu, Gruzinov and Barkana ([1])):

$$T(k) \approx \left| \frac{\cos(x^{2.7})}{1 + x^{7.5}} \right|^{\frac{3}{2}} \qquad \text{with} \qquad x = 1.61 m_{22}^{1/18} \frac{k}{k_{Jeq}}$$

This formula has been tested varying the dark matter density ($0.2 < \Omega_D \cdot h^2 < 0.4$), m_{FDM} ($0.5 < m_{22} < 25$) and the neutrino mass ($0.06\text{eV} < m_\nu < 0.6\text{eV}$) without noticing any remarkable mismatch. The only parameter that has produced a considerable effect when made to vary is the redshift ($0 < z < 1299$); however, $T(k)$ showed only a negligible dependence on the redshift for the values of our interest ($0 < z \lesssim 10$).

Another mean to test the FDM model is represented by the Lyman-alpha forest, which allows to probe the way in which FDM affects the formation of structures. After a brief explanation on how it is possible to derive a constraint on the mass of FDM particles through the forest, it has been shown that $2 \cdot 10^{-21}$ eV is a lower limit for m_{FDM}. This value clashes with the expected one and is unable to solve the small-scale crisis. The expected number of FDM subhalos for the Milky Way was derived according to $m_{22} = 25$: one of the very few values of m_{FDM} that could almost solve the missing-satellite problem while satisfying the constraint coming from the Lyman-alpha forest. This resulted in 85.7 expected subhaloes with $10^8 M_\odot/h < M_{sub} < 10^{10} M_\odot/h$: a better result than the ones produced with standard CDM models, but still incompatible with the observational data.
Mixed models are an attempt to solve this mismatch and recover the FDM model. They are based on the assumption that Dark Matter is constituted of both FDM and CDM, and every mixed model is characterized by the parameter $F = \dfrac{\rho_{FDM}}{\rho_{CDM}}$. The $T(k)$ function was tested varying F, resulting in a much smaller suppression for $F < 1$ and reproducing

the original one for $F = 1$, as expected. According to mixed models, the Lyman-alpha forest is compatible with FDM for $F \lesssim 0.4$. However, as reported in 5.3, almost none combination of F and m_{22} is able to solve the missing-satellite problem while remaining compatible with the Lyman-alpha forest and the expected value of m_{FDM}. This fact was also probed in Section 6, where the suppression of the CDM density power spectrum in the nonlinear regime over the FDM one was presented and analyzed (basically, the nonlinear analogous of $T(k)$ was derived). The suppression was studied varying the mass of FDM particles $2.5 < m_{22} < 25$ and the redshift $2 < z < 5.4$, showing a much more marked dependence of the suppression on this last parameter. Furthermore, it is possible to notice that there is less suppression than in the linear regime.

Therefore, assuming that the data produced with the simulations are correct, it is possible to conclude that the values of the FDM particles mass compatible with the Lyman-alpha forest are too large to solve the missing-satellite problem, and thus the small-scale crisis.

A possible solution could be a new model, in which the properties of Fuzzy Dark Matter depend on the redshift. In particular, the constraint on the mass given by the Lyman-alpha forest should also depend on the redshift and allow m_{FDM} values able to solve the small-scale crisis for $z \approx 0$.

APPENDIX A: A more sophisticated fit for the linear suppression

This appendix aims to further analyze the suppression of FDM power spectra over CDM ones. As reported in Section 4, the suppression is well-fitted by the function proposed by Hu, Gruzinov and Barkana:

$$T_{hgb}(k) \approx \left(\frac{\cos(x^3)}{1+x^8}\right)^2 \qquad \text{with} \qquad x = 1.61 m_{22}^{1/18} \cdot \frac{k}{9 m_{22}^{1/2} \mathrm{Mpc}^{-1}} \tag{65}$$

A first correction is provided by another choice of the exponents:

$$T_{fit}(k) \approx \left|\frac{\cos(x^{2.7})}{1+x^{7.5}}\right|^{\frac{3}{2}} \tag{66}$$

which follows more neighborly the simulation along the suppression.

However, as evidenced in Figures 17 and 18, both these formulas fail to reproduce two important aspects of the simulation:

- The local minima aren't correctly fitted.
- The relative positions of local minima of $T_{simulation}$ and T_{fit} change when mass is made to vary. This fact seems to suggest that the T function must depend on the mass not only through the definition of x.

At first, one could try to improve the fit through a different choice of the three exponents: 2.7, 7.5 and 1.5. However, the slope of the suppression is well-fitted for every tested value of m_{22}, and since it is determined solely by the exponents 7.5 and 1.5, it is reasonable to keep these values fixed. It is still possible to reproduce the same slope with a different choice of both the exponents (provided that their sum is kept fixed at -6, so that the slope is well-fitted even when the 1 in the denominator is negligible.). However, no combination of the three exponents capable to correctly interpolate all the local minima has been identified.

An interesting alternative provides that at least one of the three exponents is not constant. It is possible that the exponents external to the cosine may vary, but the constraint over their sum must be still valid. Therefore, it is likely that the only non-constant exponent is that within the cosine. This offers an opportunity to insert an additional dependence on the mass in the T function. Moreover, since the external exponents 7.5 and 1.5 proved to be a good choice, we will keep their values. To sum up, the simulation local minima could be interpolated by the general function:

$$T_{general}(k) \approx \left|\frac{\cos(x^{g(x,m_{22})})}{1+x^{7.5}}\right|^{\frac{3}{2}} \tag{67}$$

where the function $g(x, m_{22})$ possibly depends on the mass.

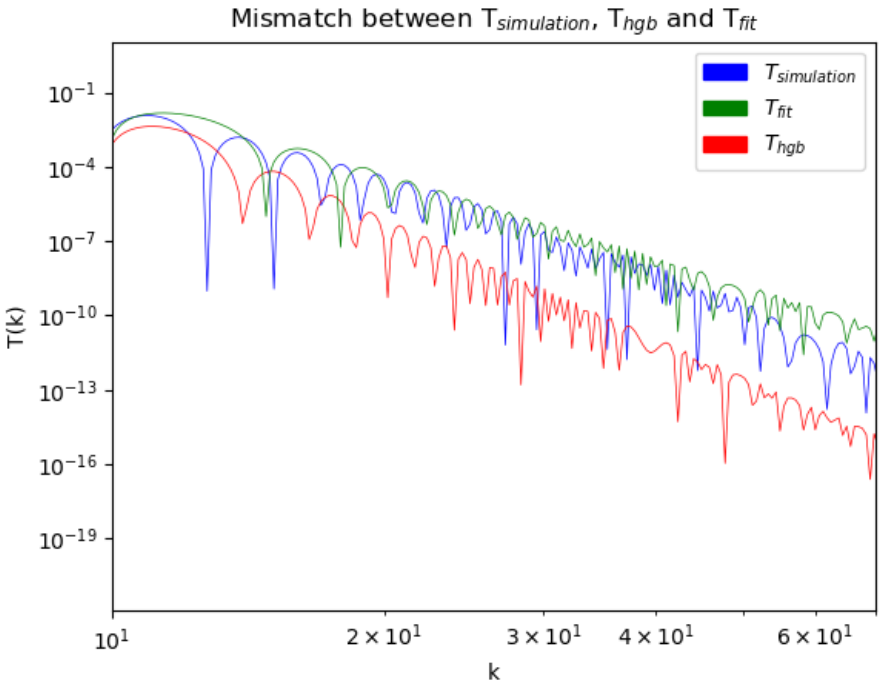

Figure 17: Comparison between the suppression of $T_{simulation}$, T_{hgb} and T_{fit} for $m_{22} = 1$. The mismatch between the position of the local minima is glaring.

The g function has been determined through the analysis of the suppression for $m_{22} = 4$ and then generalized to other values of m_{22}. The whole procedure is summarized below.

At first, the suppression has been divided into seven areas. For each area the function g was considered constant, and its value that best reproduced the position of the local minima was estimated. At the end of the process, it is possible to obtain a set of points showing the shape of the g function. g appeared to be constant for $x \gtrsim 45$ and was considered constant also before the beginning of the suppression. The results reached with this method suggest that g resembles a logistic function. In particular, a good choice for g could be:

$$g(x, m_{22}) = 3.3 - \frac{0.6}{1 + e^{-1.75\cdot(45 f(m_{22}) - x)}} \tag{68}$$

where $f(m_{22}) = x(m_{22})/k$. The explicit dependence of $T_{general}$ by f is due to the fact that the drop of $g(k)$ takes place at $k \approx 45$ for every value of m_{22}, thus a factor $45 \cdot f$ was introduced in order to express the drop in terms of $x = f \cdot k$. Therefore, the factor 45 has to be considered to have the same dimension of k: Mpc^{-1}. Thus, the expected explicit dependence of T on the mass arises. Finally, it is possible to write the proposed general fit:

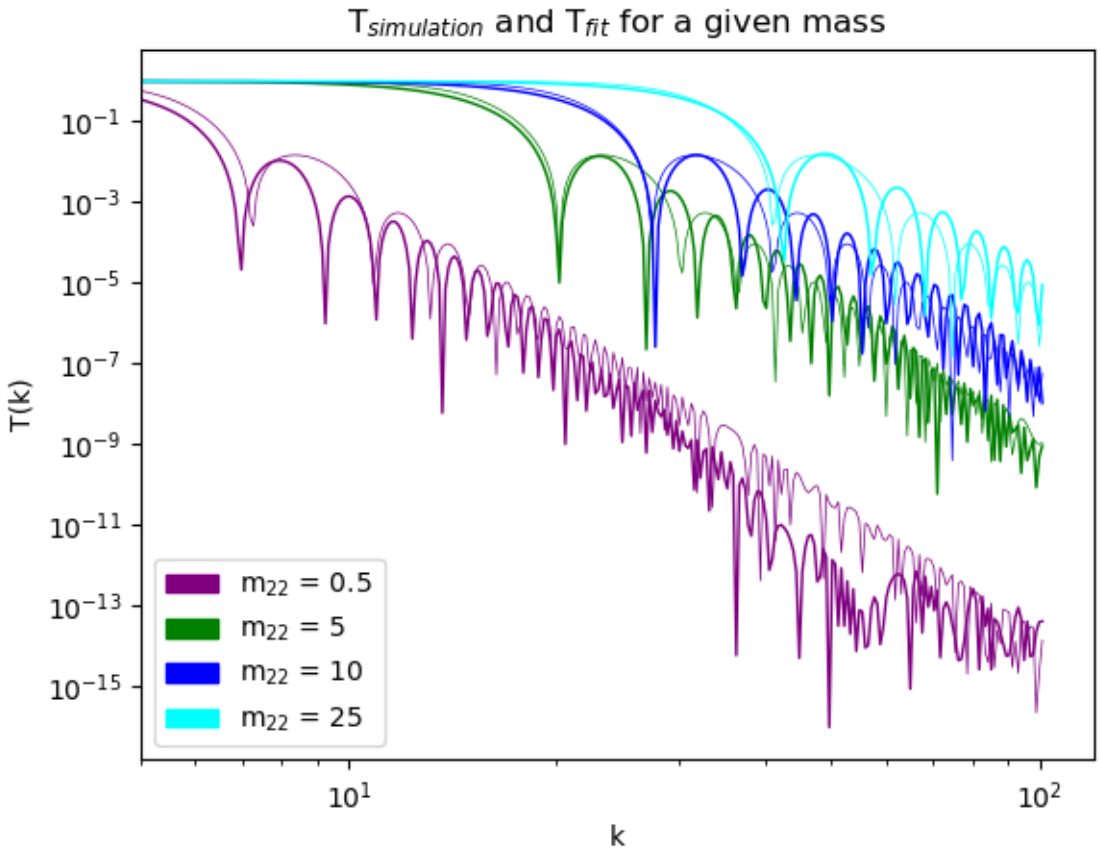

Figure 18: Comparison between the suppression of $T_{simulation}$ (bold line) and T_{fit} (thin line) for different m_{22} values. It is possible to notice, for example, that the first local minimum of the simulation precedes the one of T_{fit} for $m_{22} = 0.5$, while their roles are reversed for $m_{22} = 25$. The same consideration applies to all the other minima.

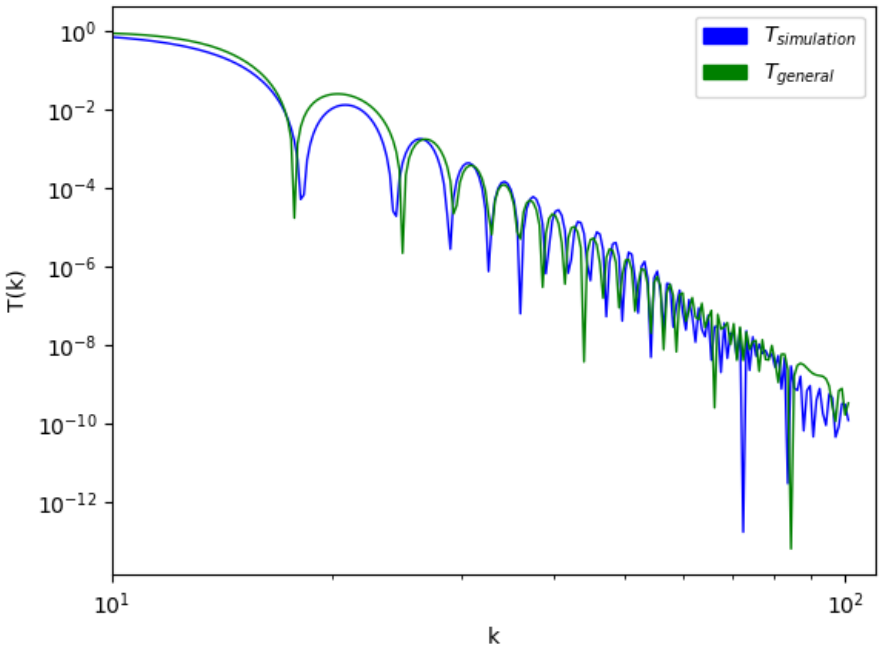

Figure 19: A comparison between the suppression calculated through simulations and $T_{general}$.

$$T(x) = \left| \frac{\cos\left(x^{3.3-\frac{0.6}{1+e^{-1.75*(45\cdot f-x)}}}\right)}{1+x^{7.5}} \right|^{1.5} \tag{69}$$

which is compared with the simulation for $m_{22} = 4$ in Figure 19.

The rapid variation of the g function between the intervals in which it is substantially constant could be interpreted as the consequence of a phenomenon that occurs only when k exceeds a certain value. Otherwise, it could be a non-physical numerical consequence of the algorithm followed to generate power spectra.

APPENDIX B: AX-GADGET

In Section 23, the Madelung equations, together with the modified Navier-Stokes equation, were presented as a handier mean to produce numerical simulations involving CDM.

$$\dot{\rho} + 3H\rho + \frac{1}{R}\nabla \cdot (\rho \mathbf{v}) = 0$$
$$\dot{\mathbf{v}} + H\mathbf{v} + \frac{1}{R}(\mathbf{v} \cdot \nabla)\mathbf{v} = -\frac{1}{R}\nabla\Phi + \frac{\hbar^2}{2R^3m^2}\nabla\left(\frac{\nabla^2\sqrt{\rho}}{\sqrt{\rho}}\right)$$

where the gravitational potential satisfies the Poisson equation:

$$\nabla^2\Phi = 4\pi G a^2 \rho_b \delta$$

where $\delta = (\rho - \rho_b)/\rho_b$ is the density fluctuation around the background density ρ_b.

The simulations were analyzed in both the linear and nonlinear regime, but while for the first case the well-known CAMB code was used, analysis in the nonlinear regime required the use of AX-GADGET: a new module of the parallel N-Body code P-GADGET3. In this Appendix, the basic concepts underlying the functioning of AX-GADGET will be illustrated.

The pressure term P can be related to ρ through an equation of state ([37]):

$$P = \frac{\lambda\rho^2}{2m^2}$$

where m and λ represents the mass of FDM particles and the self-interaction coupling constant of the field. In this terms, it is possible to derive the form of the Quantum Pressure Q:

$$Q = \frac{\hbar^2}{2m^2}\frac{\nabla^2\sqrt{\rho}}{\sqrt{\rho}} = \frac{\hbar^2}{2m^2}\left(\frac{\nabla^2\rho}{2\rho} - \frac{|\nabla\rho|^2}{4\rho^2}\right) \tag{70}$$

These equations have a stable solution for $\delta = \Phi = |\mathbf{v}| = 0$, and assuming that $\delta, \Phi, |\mathbf{v}| \ll 1$ it is possible to derive a set of *linearised* equations:

$$\ddot{\delta} + 2H\dot{\delta} + \left(\frac{\hbar^2k^4}{4m^2a^4} + \frac{c_s^2k^2}{a^2} - \frac{4\pi G\rho_b}{a^3}\right)\delta = 0 \tag{71}$$

where $\delta(\mathbf{x}, t)$ has been decomposed in Fourier modes $\delta_k e^{i\mathbf{k}\cdot\mathbf{x}}$ and $c_s^2 = \partial_\rho P(\rho)|_{\rho_b}$ is the sound speed of the fluid.

The functioning of AX-GADGET is well exemplified by the way it computes of the Quantum Pressure effects. Therefore, it will be assumed that $\lambda = c_s = 0$ henceforth.

A perturbed stable solution of (71) is given by a δ with mode:

$$k_Q(a) = \left(\frac{16\pi G\rho_b a^3 m^2}{\hbar^2}\right)^{1/4} a^{1/4}$$

and wavelength $\lambda_Q = 2\pi/k_Q$ (which represents a quantum version of the Jeans wavelength: the scale at which gravity is perfectly balanced by the Quantum Pressure effect).

More in general, the solution of (71) is a linear combination of two modes: a growing one D_+ and a decaying one D_-.

$$D_+(x) = \frac{(3-x^2)\cos x + 3x \sin x}{x^2}$$
$$D_-(x) = \frac{(3-x^2)\sin x - 3x \cos x}{x^2}$$
$$\text{with} \qquad x(k,a) = \sqrt{6}\frac{k^2}{k_Q^2(a)}$$

The presence of a growing mode is crucial because, as shown in the following, it makes the linear approximations of (71) potentially inaccurate. In fact, since $k_Q(a) \propto a^{(1/4)}$ increases with time, oscillating modes start growing as soon as they are passed by the quantum Jeans scale, each at a different redshift. However, while in linear approximation the fastest growth of density perturbations is indeed linear $D_+ \propto a$ (thus, intermediate suppressed scales won't ever be comparable to the largest ones), in the nonlinear regime, where intermediate and small scales grow faster at low redshift, different scales are coupled. For this reason, it is necessary to develop numerical techniques to compute hydrodynamical N-Body simulations in the nonlinear regime.

The tool that accomplishes this task is the AX-GADGET code, which exploits the so-called Smoothed-Particle Hydrodynamics (SPH) techniques to compute the Quantum Pressure acceleration and the corresponding Navier-Stokes equation. The SPH method idea is to divide the fluid into a set of discrete elements, referred to as particles. These particles have a spatial distance (known as the *smoothing length*), over which their properties are "smoothed" by a *kernel function*, which can take many possible values. This means that the physical quantity of any particle can be obtained by summing the relevant properties of all the particles that lie within the range of the kernel. Therefore, the value of a certain observable O at the position of particle i is expressed as the sums of its value over all the neighbouring particles ($NN(i)$):

$$O_i = \sum_{j \in NN(i)} m_j \frac{O_j}{\rho_j} W_{ij}$$

where m_j is the mass, ρ_j the density and W_{ij} the kernel function. In particular, the kernel function used by AX-GADGET (and by P-GADGET3 too) is:

$$W(r,h) = \begin{cases} 1 - 6\left(\frac{r}{h}\right)^2 + 6\left(\frac{r}{h}\right)^3, & \text{if } 0 < r < h/2 \\ 2\left(1 - \frac{r}{h}\right)^3, & \text{if } h/2 < r < h \\ 0, & \text{otherwise} \end{cases}$$

where r is the distance between particles and h is the smoothing length, which is varied at each timestep remaining compatible with

$$\frac{4}{3}\pi h_i^3 \rho_i = \sum_{j \in NN(i)} m_j = M$$

So that its corresponding (spherical) region encloses enough fluid particles to match the given mass M. However, the definition of the derivative and the Laplacian of O_i is not as simple as the definition of O_i. In fact, if one chose the most natural definition for the derivative:

$$\nabla O_i = \sum_{j \in NN(i)} m_j \frac{O_j}{\rho_j} \nabla W_{ij}$$

which is not necessarily null for constant values of O_i, due to the kernel function. A second possibility is to define:

$$\nabla O_i = \sum_{j \in NN(i)} m_j \frac{O_j - O_i}{\rho_j} \frac{\Theta_j}{\Theta_i} \nabla W_{ij}$$

which is null for constant values of O, regardless the form of the differentiable function Θ. According to the most common choices for Θ, the derivative of the density field takes this form:

$$\nabla \rho_i = \sum_{j \in NN(i)} m_j \nabla W_{ij} (\rho_j - \rho_i) \begin{cases} 1/\rho_i, & \text{if } \Theta = 1 \\ 1/\rho_j, & \text{if } \Theta = \rho \\ 1/\sqrt{\rho_i \rho_j}, & \text{if } \Theta = \sqrt{\rho} \end{cases}$$

It is possible to select all these forms of Θ as input for AX-GADGET.

Another issue affects the definition of the Laplacian, which can't be in the most natural form:

$$\nabla^2 O_i = \sum_{j \in NN(i)} m_j \frac{O_j}{\rho_j} \nabla^2 W_{ij}$$

because this definition leads to unstable results, due to their high dependence on the irregularities of the particle distribution. A handier form for $\nabla^2 O$ can be obtained following the same approach as before:

$$\nabla^2 O_i = \sum_{j \in NN(i)} m_j \frac{O_j - O_i}{\rho_j} \frac{\Theta_j}{\Theta_i} \nabla^2 W_{ij} - \frac{2}{\Theta_i} \nabla O_i \cdot \nabla \Theta_i$$

These definitions make it possible to estimate the value of the Quantum Pressure acceleration which, since it is proportional to a third order derivative of the density field, needs three cycles of computation to be determined. The first aims to calculate the density:

$$\rho_i = \sum_{j \in NN(i)} m_j W_{ij}$$

the second one leads to its gradient and Laplacian:

$$\nabla \rho_i = \sum_{j \in NN(i)} m_j \nabla W_{ij} \frac{\rho_j - \rho_i}{\sqrt{\rho_i \rho_j}} \nabla^2 \rho_i = \sum_{j \in NN(i)} m_j \nabla^2 W_{ij} \frac{\rho_j - \rho_i}{\sqrt{\rho_i \rho_j}} - \frac{|\nabla \rho_i|^2}{\rho_i}$$

FInally, it is possible to build the Quantum Pressure term using equation (70):

$$\nabla Q_i = \frac{\hbar^2}{2m^2} \sum_{j \in NN(i)} \frac{m_j}{f_j \rho_j} \nabla W_{ij} \left(\frac{\nabla^2 \rho_j}{2\rho_j} - \frac{|\nabla \rho_j|^2}{4\rho_j^2} \right)$$

where factors f_i are introduced to enforce the condition (7)

Bibliography

References

[1] W. Hu, R. Barkana, and A. Gruzinov, "Fuzzy Cold Dark Matter: the wave properties of ultralight particles", Phys. Rev. Lett. **85** 1158 (2000).

[2] L. Ham, J.P. Ostriker, S. Tremaine, and E. Witten, "Ultralight scalars as cosmological dark matter", Phys. Rev. D **95**, 043541 (2017).

[3] A. Arvanitaki, S. DImopoulos, S. Dubovsky, N. Kaloper, and J. March-Russel, "String axiverse", Phys. Rev. D **81**, 123530 (2010).

[4] J.E. Kim and D.J.E. Marsh, "An ultralight pseudoscalar boson", Phys. Rev. D **93**, 025027 (2016).

[5] A. Khmelnitsky and V. Rubakov, "Pulsar timing signal from ultralight scalar dark matter", J. Cosmol. Astropart. Phys. 02 019 (2014).

[6] L.M. Widrow and N. Kaiser, "Using the Schrödinger equation to simulate collisionless matter", The Astrophys. J. **416**, L71 (1993).

[7] S.-R. Chen, H.-Y. Schive, and T. Chiueh, "Jeans analysis for dwarf spheroidal galaxies in wave dark matter", arXiv:1606.09030 (2016).

[8] J.F. Navarro, C.S. Frenk, and S.D.M. White, "A universal density profile from hierarchical clustering", Astrophys. J. **490**, 493 (1997).

[9] B. SChwabe, J.C.Niemeyer, and J.F.Engels, "Simulations of solitonic core mergers in ultralight axion dark matter cosmologies", Phys. Rev. D **94**, 043513 (2016).

[10] J. Binney and S. Tremaine, *Galactic Dynamics* 2nd ed. (Princeton University Press, Princeton, NJ, 2008).

[11] J. Binney and S. Tremaine, "Galactic Dynamics" 2nd ed. (Princeton University Press, Princeton, NJ, 2008).

[12] J.-W. Lee and S. Lim, "Minimum mass og galaxies from BEC or scalar field dark matter", J. Cosmol. Astropart. Phys. 1 (2010).

[13] W.J.G. De Block, "The core-cusp problem", arXiv:0910.3538v1 (2009).

[14] H. Deng, M. P. Hertzberg, M. H. Namjoo, and A. Masoumi, "Can Light Dark Matter Solve the Core-Cusp Problem?", arXiv:1804.05921v1 (2018).

[15] J.F. Navarro, V.R. Eke, and C.S. Frenk, "The cores of dwarf galaxies haloes", Mon. Not. R. Astron. Soc. **283**, L72-L78 (1996).

[16] A. Burkert, "The structure of dark matter haloes in dwarf galaxies", Astrophys. J. **447**, L25 (1995).

[17] Wolfram Research, Inc., Mathematica version 11.3, Champaign, Illinois (2018).

[18] I. Ferrero, M.G. Abadi, J.F. Navarro, L.V. Sales, and S. Gurovich, "The dark matter halos of dwarf galaxies: a challenge for the ΛCDM paradigm?", arXiv:1111.6609v3 (2012).

[19] A. A. Klypin, A. V. Kravtsov, O. Valenzuela, and F. Prada, "Where are the missing Galactic satellites?", Astrophys. J. **522**, 82 (1999).

[20] Y.D. Hezaveh, N. Dalal, D.P. Marrone, Y.-Y. Mao, W.Morningstar, D. Wen, R.D.Blandford, J.E. Carlstrom, C.D. FAssnacht, G.P.Holder, A. Kemball, P.J. Marshall, N. Murray, L.P.Levasseur, J.D. Vieira, and R.H.Wechsler, "Detection of lensing substructure using ALMA obesrvations of the dusty galaxy SDP.81", Astrophys. J. **823**, 37 (2016).

[21] M- Boylan-Kolchin, J.S. Bullock, and M. Kaplinghat, "Too big to fail? The puzzling darkness of massive Milky Way subhaloes", Mon. Not. R. Astron. Soc. **415**, L40 (2011).

[22] A. Lewis, "Efficient sampling of fast and slow cosmological parameters", Phys. Rev. **D87** 103529 (2013).

[23] A. Lewis, *CAMB notes*, http://cosmologist.info/CITA/IoA/Sussex (2014).

[24] R. Hlozek, D. Grin, D.J.E. March, P.G. Ferreira, "A search for ultralight axions using precision cosmological data", arXiv:1410.2896v2 (2015)

[25] P.S. Corasaniti, S. Agarwal, D.J.E. Marsh, and S. Das, "Constraint on dark matter scenarios from measurements of the galaxy luminosity function at high redshifts", arXiv:1611.05892 (2017).

[26] V.K. Narayanan, D.N. Spergel, R. Davé, C.-P. Ma, "Lyman-alpha forest constraints on the mass of warm dark matter and the shape of the linear power spectrum", arXiv:astro-ph/0005095v1 (2000).

[27] V. Irŝiĉ, M. Viel, M. G. Haehnelt, J.S. Bolton, G.D. Becker "First constraints on fuzzy dark matter from Lyman-α forest data and hydrodynamical simulations", arXiv:1703.04683v2 (2017).

[28] T. Kobayashi, R. Murgia, A. De Simone, V. rŝiĉ, and M. Viel, "Lyman-α constraints on ultralight scalar dark matter: implications for the early and late universe", arXiv:1708.00015v1 (2017).

[29] A. Schneider, R. E. Smith, D. Reed, "Halo mass function and the free streaming scale", MNRAS **433**, 1573 (2013).

[30] W. H. Press, P. Schechter, "Formation of Galaxies and Clusters of Galaxies by Self-Similar Gravitational Condensation", Astrophys. J. **187**, 425 (1974).

[31] A. Schneider, "Structure formation with suppressed small-scale perturbations", arXiv:1412.2133v2 (2015).

[32] H. Mo, F.C. van den Bosch, S. White, *Galaxy formation and evolution* (Cambdrige University Press, Cambridge, UK, 2010)

[33] R. K. Sheth, G. Tormen, "Large-scale bias and the peak background split", MNRAS **308**, 119 (1999).

[34] E. Bertschinger, "On the Growth of Perturbations as a Test of Dark Energy", Astrophys. J. **648**, 797 (2006).

[35] C. Lacey and S. Cole, "Merger rates in hierarchical models of galaxy formation", MNRAS **262**, 627 (1993)

[36] C. Giocoli, G. Tormen, F. C. van den Bosch, "The population of dark matter subhaloes: mass functions and average mass-loss rates", MNRAS **386**, 2135 (2008).

[37] M. Nori, M. Baldi, "AX-GADGET: a new code for cosmological simulations of fuzzy dark matter and axion models", arXiv:1801.08144v1 (2018).

[38] Pylians libraries, https://github.com/franciscovillaescusa/Pylians